Rodrigo Cassio de Barros

Lifetime Evaluation of Multifunctional Single-Phase PV Inverter During Harmonic Current Compensation

Belo Horizonte, MG

2019

Rodrigo Cassio de Barros

Lifetime Evaluation of Multifunctional Single-Phase PV Inverter During Harmonic Current Compensation

Dissertação de mestrado submetida à banca examinadora designada pelo Colegiado do Programa de Pós-Graduação em Engenharia Elétrica do Centro Federal de Educação Tecnológica de Minas Gerais e da Universidade Federal de São João Del Rei, como parte dos requisitos necessários à obtenção do grau de Mestre em Engenharia Elétrica.

Orientador: Prof. Dr. Heverton Augusto Pereira

Belo Horizonte, MG

2019

Barros, Rodrigo Cassio de
B277l Lifetime evaluation of multifunctional single-phase PV inverter during harmonic current compensation / Rodrigo Cassio de Barros. – 2019.
78 f.: il., gráfs, tabs.

Dissertação de mestrado apresentada ao Programa de Pós-Graduação em Engenharia Elétrica em associação ampla entre a UFSJ e o CEFET-MG.
Orientador: Heverton Augusto Pereira.
Banca examinadora: Heverton Augusto Pereira, Wallace do Couto Boaventura e Marcelo Martins Stopa.
Dissertação (mestrado) – Centro Federal de Educação Tecnológica de Minas Gerais.

1. Sistemas de energia fotovoltaica – Teses. 2. Harmônicos (ondas elétricas) – Teses. 3. Ciclo de vida do produto – Teses. I. Pereira, Heverton Augusto. II. Centro Federal de Educação Tecnológica de Minas Gerais. III. Universidade Federal de São João del-Rei. IV. Título.

CDD 621.31244

Elaboração da ficha catalográfica pela Biblioteca-Campus II / CEFET-MG

Rodrigo Cassio de Barros

Lifetime Evaluation of Multifunctional Single-Phase PV Inverter During Harmonic Current Compensation

Dissertação de mestrado submetida à banca examinadora designada pelo Colegiado do Programa de Pós-Graduação em Engenharia Elétrica do Centro Federal de Educação Tecnológica de Minas Gerais e da Universidade Federal de São João Del Rei, como parte dos requisitos necessários à obtenção do grau de Mestre em Engenharia Elétrica.

Trabalho aprovado em 03 de Maio de 2019.

COMISSÃO EXAMINADORA

Prof. Dr. Heverton Augusto Pereira
Orientador

Prof. Dr. Wallace do Couto Boaventura
Convidado 1

Prof. Dr. Marcelo Martins Stopa
Convidado 2

Belo Horizonte, MG
2019

À minha família, mentores e amigos.

Agradecimentos

Primeiramente, obrigado a Deus e aos meus pais, José Maria e Gurdiana, pelo suporte incondicional. Obrigado por ensinarem que humildade e dedicação as maiores armas que posso ter. Aos meus irmãos Tiago, Thais e Candido por sempre me apoiarem e conceder o calor do amor fraternal. Aos meus cunhados, Ana Claudia e Wesley, por serem tão atenciosos e presentes. A minha sobrinha e afilhada Helena, por trazer tanta luz. Aos meus avós, tios(as), primos(as) e a todos os amigos que contribuíram para essa conquista. Ao grupo de pesquisa GESEP por todo o suporte durante essa caminhada. Aos meus amigos de trabalho pelo companheirismo, amizade e cumplicidade. Ao meu orientador, Prof. Heverton, pela paciência e boa vontade de ensinar. Ao Prof. Erick Brito, por ter um papel fundamental na construção deste trabalho. Ao programa de pós graduação em Engenharia Elétrica do CEFET e a CAPES.

"All we have to decide is what to do with the time that is given to us."
(Gandalf)

Resumo

A qualidade da energia da rede elétrica do ponto de vista de poluição harmônic está sendo comprometida nas últimas décadas devido ao aumento das unidades de microgeração distribuída e das cargas não lineares conectadas à rede. Neste contexto, inversores fotovoltaicos (FV) multifuncionais têm sido descritos como uma plausível solução para a melhoria na qualidade de energia. A ideia principal é usar o inversor FV para serviços auxiliares, como compensação de corrente harmônica. Portanto, é necessário verificar o quanto esta extra funcionalidade pode afetar a vida útil do inversor fotovoltaico. No entanto, essa tarefa não é simples, uma vez que a corrente do inversor apresenta diferentes comportamentos dependendo da componente harmônica que está sendo compensada. Além disso, com a metodologia atualmente disponível na literatura, a estimativa do consumo de vida útil do inversor FV seria complexa, uma vez que se considera apenas a injeção da componente fundamental da corrente na rede elétrica. Assim, este trabalho propõe uma metodologia de estimativa de vida útil, que considera o efeito de qualquer componente harmônica durante o processo de compensação. Além disso, as perdas de condução e chaveamento de um IGBT durante o processo de compensação de corrente harmônica é modelado neste trabalho. A estimativa de vida útil é realizada considerando-se um inversor FV de 5kW, no qual observou-se a dependência da mesma em relação à componente harmônica, à corrente fundamental, à ordem harmônica e ao ângulo de fase.

Palavras-chaves: Inversor FV, Operação Multifuncional, Compensação de Corrente Harmônica, Estimativa de Vida Útil.

Abstract

The grid power quality has been compromised in recent decades due to the increasing of nonlinear load and distribution generation units connected to the power system. In this scenario, multifunctional Photovoltaic (PV) inverters have been described as a suitable power quality solution. The basic idea is using the PV inverter for ancillary services, such as the harmonic current compensation. Therefore, it is necessary to verify how much this extra functionality can affect the lifetime of the PV inverter. However, this task is not straightforward, since the inverter current presents different behaviors depending on the compensated harmonic component. In addition, with the methodology currently available in the literature, the lifetime consumption of the PV inverter would be complex, since it considers only the injection of fundamental current into the grid. Thus, this work proposes a lifetime consumption methodology, which considers the effect of any harmonic component on the lifetime consumption during the harmonic current compensation process. In addition, the conduction and switching power losses of an IGBT during the harmonic compensation process is modeled in this work. Furthermore, the lifetime evaluation is carried out considering a 5kW PV inverter and it is concluded that its lifetime consumption depends on the relationship between the harmonic component, the fundamental current, the harmonic order and phase angle.

Key-words: PV Inverter, Multifunctional Operation, Harmonic Current Compensation, Lifetime Evaluation.

List of Figures

List of Tables

List of abbreviations and acronyms

ANEEL	*Agência Naconal de Energia Elétrica*
CEFET	*Centro Federal de Educação Tecnológica de Minas Gerais*
CTE	Coefficient Thermal Expansion
FV	*Fotovoltaico*
HCC	Harmonic Current Compensation
IEEE	Institute of Electrical and Electronics Engineering
IGBT	Insulated Gate Bipolar Transistors
LC	Lifetime Consumption
MPPT	Maximum Power Tracking
PCC	Point of Common Coupling
PI	Proportional Integral
PLL	Phase Locked Loop
PMR	Proportional Multi-Resonant
PV	Photovoltaic
PWM	Pulse Width Modulation
SFR	Synchronous Reference Frame
SOGI	Second-Order-Generalized-Integrator
SS	Steady State
THD	Total Harmonic Distortion

List of symbols

C_1	Capacitance value (from the boost converter)
C_2	Capacitance value (from the dc-link capacitor)
C_f	Capacitance value (from the LCL filter)
$C_{n(h-a)}$	Thermal capacitance
i_c	IGBT collector current rate
I_{cn}	IGBT collector current in nominal operation
i_g	Grid current
i_{PV}	Current generated by the PV array
i_s	Inverter output current
I_f	Fundamental current amplitude
I_h	Harmonic current amplitude
i_{ind}	Inductor current (from the boost converter)
i_L	Load current
i_{rrn}	Diode nominal reverse current of diode
f_o	Electrical grid frequency
h	Harmonic order
v_a	Inverter output voltage
v_{ce}	IGBT collector-to-emitter rate
V_{cen}	IGBT collector-to-emitter voltage in the nominal operation
v_{dc}	dc-link voltage
V_{cen_0}	IGBT on stage zero current collector-to-emitter voltage
V_g	Grid voltage
v_{PCC}	Voltage at the point of common coupling

v_{PV}	Voltage generated by the PV
L_f	Inductance value (from the LCL filter)
L_g	Inductance value (from the LCL filter)
L_{ind}	Inductance value (from the boost converter)
m	Modulation index
P_{out}	Output power generation from the PV array.
Q_{rr}	Diode reverse recovery charge
R_{100}	Approximated line equation for T_j equal to 100 °C
$R_{eq(c-h)}$	Junction to case thermal resistance
$R_{eq(h-a)}$	Heat sink to ambient thermal resistance.
T_j	IGBT junction temperature
T_s	Switching period
T	Grid period
t_{on}	IGBT temperature heating time
t_{rn}	Nominal rising time
t_{rrn}	Diode nominal reverse time
w_f	Fundamental frequency.
w_h	Harmonic frequency.
ΔT_j	IGBT fluctuation junction temperature
δ	Duty cycle
θ_h	Harmonic phase angle

Contents

1 Introduction

Power system harmonics are receiving a great deal of attention due to the increasing penetration of nonlinear loads connected to the point of common coupling (PCC) (LIANG; BIN-KARIM, 2018). These loads inject harmonic current components multiple of the grid frequency (50/60 Hz) into the distribution network. In residential and industry voltage level are found the largest concentration of nonlinear loads, such as, advanced power conversion devices, electronic equipment, computers, office automation, air-conditioning systems, compact fluorescent lamps, etc (GHORBANI, 2011; SMITH, 2002). The harmonic components injected by an unique nonlinear load are usually too small to cause considerable harmonic current distortion in a distribution power systems. However, when operating in large numbers, the total effect has the potential to cause serious harmonic distortion levels.

The increasing of the current harmonic distortion can bring serious problems to the power system, including overheating in transformers, capacitors, motors and generators. In addition, it can cause error in the measurement devices and fault in protection systems (FILHO et al., 2016). Also, nonlinear loads can cause significant costs to the distribution system, since there are power losses dissipation due to the harmonic current and the reduction of the electrical equipment reliability. In face of this issue, harmonic disturbance has been strongly discussed, since costumers and utilities companies need to maintain a certain level of harmonic distortion at the PCC. One of the most used parameter limits for the total harmonic distortion THD are ruled by IEEE standard (IEEE-STD, 2014), which the THD limits for systems rated in 120 V through 69 kV and above than 69 kV.

In this context, there are some works in the literature which discuss the financial impact of the harmonic distortion. Reference (ASHOUR; YOUSSEF, 2005) considers ten case studies in the Alexandria electricity distribution company, located in Egypt. In the worth case, the extra costs due to the harmonic component was estimated in 3.25 million dollars/year. Reference (KEY, 1995) gives estimation of harmonic related losses in an office building. In this case, about 60 kW electronic loads (mainly computers) are connected and they operate 12 hours per day for 365 days in one year. It was found from the analysis that those offices were paying extra energy bills of 2100 dollars in each year. These two studies do not consider the financial losses due to the lifetime reduction of the equipment.

There are some devices available in the literature to mitigate harmonic components caused by nonlinear loads. Line reactors are considered the cheapest solution (SCHWANZ; BOLLEN; LARSSON, 2016). However, they present voltage drop and increase the system power losses. Isolation and K- factor transformers are also used (SEKAR; RABI, 2012). Even though this solutions achieve effective harmonic attenuation, they increase the cost and the power losses of the power system. Nevertheless, passive filters have been used (SHI et al., 2017). This technique presents simple design, low cost and high efficiency. However, passive filters bring resonant issues to the power system, since they are tuning for fixed frequency and have large size. Other solution are active filters (DASH; PAIKRAY; SWAIN, 2017), which do not present resonant issues, and they can be used to mitigate a largest rate of harmonic components. On the order hand, active filters are considered expensive and they require a complex control system.

In this scenario, multifunctional photovoltaic (PV) inverters have been strongly discussed as a sustainable solution to harmonic current mitigation (NERKAR; DHAMAL; SINHA, 2016; YANG et al., 2016). The increase of the of distributed generation (DG) based on PV solar energy has encourage to use the PV inverter to provide ancillary services. According to ANEEL, in 2018, PV solar systems reached 99% of the total installations number classified as distributed micro and mini-generation. The PV systems reached 181.8 MW in terms of accumulated installed power until May of 2018.

The basic idea is using the PV inverter to provide ancillary services when it is operating bellow the nominal active power conditions. As shown in Figure 1, the PV inverter works only around 30% of its capacity during the day. Therefore, the PV system are expected to be more controllable and to operate with high efficiency. Thus, the PV inverter can make a better use of the available excess capacity in order to improve the grid power quality. The main ancillary services are highlighted: reactive power injection, harmonic current compensation and frequency regulation (L.XAVIER, 2018).

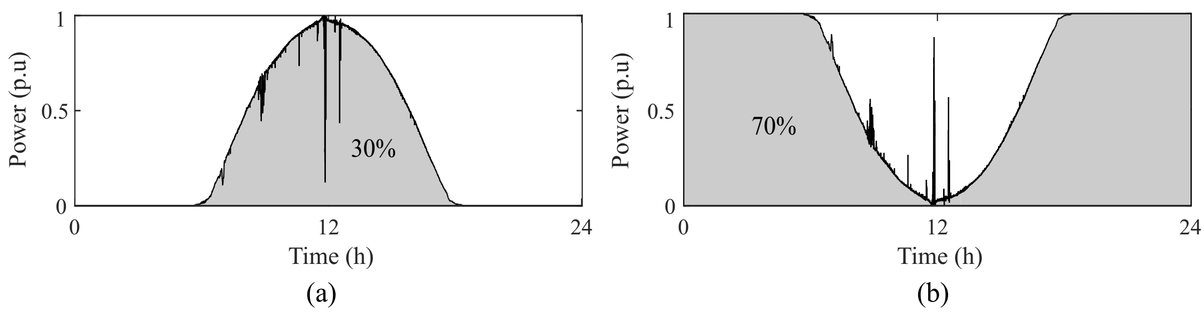

Figure 1 – (a) PV inverter injecting active power into the grid, which represent 30% of its capacity. In (b) represents the PV inverter excess capacity, which represents 70 % (L.XAVIER, 2018).

However, when grid-connected PV systems provide ancillary services, the reliability of the power PV inverter needs to be addressed (ANURAG; YANG; BLAABJERG, 2015). Depending on the grid distortion level and environmental conditions, the PV inverter is exposed to different stresses and efforts, which directly affect its lifetime consumption (FALCK et al., 2018). Therefore, in order to analyze the multifunctional PV inverter as a cost effective solution, it is needed to quantify how much these extra services affect the PV system reliability.

1.1 PV Inverter Lifetime Evaluation

According to (FALCK et al., 2018), a survey was applied to a group of power electronic manufactures, and it was reported that more than 60% of the PV inverters failure from 10 to 20 years. Nevertheless, the cost associated with the inverter failures is around 59% of the total system cost (GOLNAS, 2013).

In this context, the PV inverter reliability is provided based on the power electronic components which present the highest failure rates inside the inverter. A survey research was applied to electronic manufactures in order to indicate the device which is considered the main target that need to be addressed by future PV inverter reliability researches (FALCK et al., 2018). As observed in Figure 2, the semiconductor device was the most addressed component.

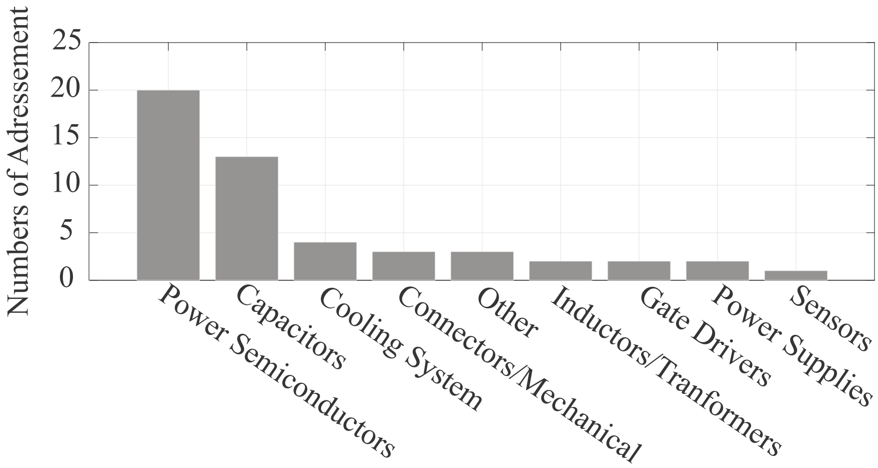

Figure 2 – Results from a survey applied to a group of power electronic manufactures with the following question: “Please indicate which components you consider most important to be addressed by future researches to improve the reliability of power electronics converter systems?”(FALCK et al., 2018).

In PV inverter applications, the insulated gate bipolar transistors (IGBT) are highly used as the semiconductor power device. They are three-terminal component used in the electronic switching process. According to previous works, power cycling and steady-state temperature have the most significant impact on the failure mechanisms of power semiconductor (FERREIRA et al., 2017), (BLAABJERG et al., 2013). These conclusions are explained based on the IGBT structure, since they are made by several layers with different materials and consequently different coefficient thermal expansion (CTE). In this context, bond wire lift-off and solder fatigue are reported the most frequently failures mode in the IGBT (ZHOU, 2010), (KEXIN et al., 2014). The bond wire lift-off happens due the mismatch of CTE, causing the crack growth at the bond wire/chip interface. The solder fatigue is due to the solder joints cracking under the chip.

In order to introduce the main concepts about the lifetime evaluation, it is important to list the origin of the power cycling which cause thermal stress in the semiconductor device (REIGOSA, 2014). There are three different power cycling listed in the literature, as follow:

- *Power cycling due to the environments disturbances*: In a real field operation conditions, the variation of solar irradiance and ambient temperature causes thermal stress in the semiconductor device.
- *Power cycling due to the grid frequency*: The temperature inside the power module device has a periodic behavior with the same frequency of the electrical grid. This power cycling highly influences in the the PV inverter lifetime evaluation.
- *Power cycling due to the power device switching frequency*: The switching frequency (f_s) also produces thermal stress in the semiconductor device. However, this thermal stress, compared to the first two items, does not cause considerable damage in the semiconductor device.

Nevertheless, as proposed in references (REIGOSA et al., 2016; MA et al., 2015), the semiconductor device lifetime consumption in the PV inverter is estimated considering two constant times: long-term and short-term. The long-term considers the damage caused by the power cycling due to environmental disturbances (REIGOSA et al., 2016). On the other hand, the short-term considers the damage caused by the power cycling due the line frequency (50/60 Hz) (MA et al., 2015). In this context, the Physics-of-failure (PoF) (MA; WANG; BLAABJERG, 2016) becomes a consolidated technique in the literature in order to understand the mechanisms which cause failure in the power devices. Thus, PoF takes into account the load profiles considering the stress that occurs in the real field operation (MA et al., 2015; SANGWONGWANICH et al., 2018).

Nevertheless, there is a gap in the literature discussing the PV inverter lifetime evaluation when it is performing ancillary services. References (ANURAG; YANG; BLAABJERG, 2015; GANDHI et al., 2018) have evaluated the life consumption when the PV inverter is compensating reactive power and the results are compared to a traditional PV inverter. In reference (YANG et al., 2017), optimal analysis between the energy production and the lifetime inverter is provided.

With regarding to the harmonic current compensation (HCC) operation mode, there are no work providing this study so far. In addition, the performance of the short-term is challenging since the current generated by the inverter presents harmonic components, which inserts additional power cycling to the power losses and consequently to the power device junction temperature, as observed in Figure 3. Furthermore, this additional power cycling is directly dependent of the harmonic order, amplitude, and phase angle, which makes necessary an adaptive lifetime evaluation methodology.

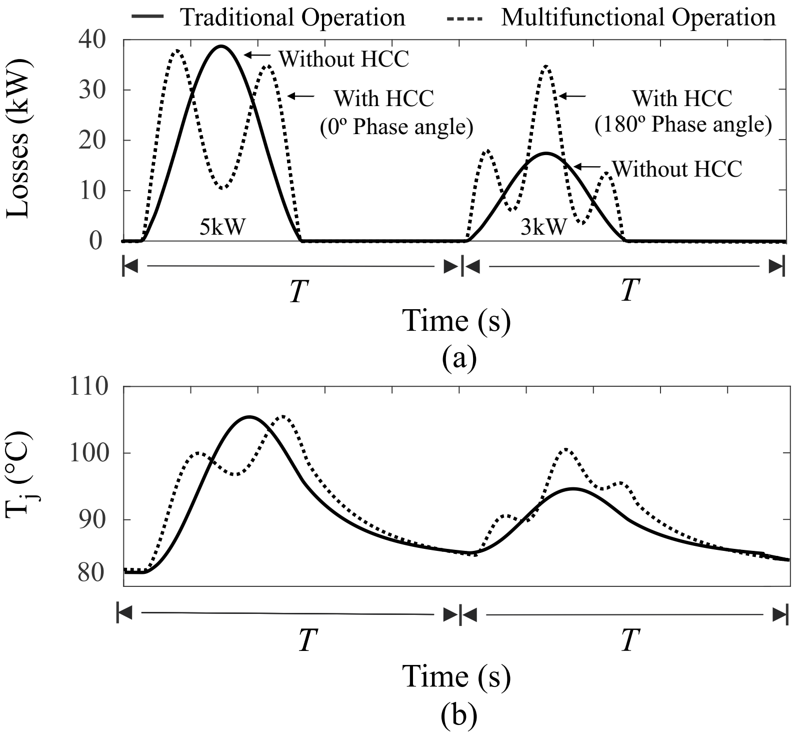

Figure 3 – Multifunctional PV inverter injecting 5 kW and 3 kW of active power and compensating 5 A of the 3^{rd} harmonic component with phase 0° and 180°. In (a), the total power losses dissipated in the semiconductor device are represented. In (b), the junction temperature waveforms are represented.

1.2 Motivation and Objectives

The multifunctional PV inverter enables a more effective PV installation, since it can make a better use of the equipment capability in order to improve the grid power quality. In this scenario, the reliability of the power electronic devices need to be addressed. The extra functionality of the PV inverter can affect the reliability of the entire PV system. Depending of grid distortion level and environmental conditions, the PV inverter is exposed to different stresses and efforts, which directly affect its lifetime consumption. Therefore, in order to analyze the multifunctional PV inverter as a cost effective solution, it is needed to quantify how much these extra functionality affects the reliability of the PV system.

Since there are no work in the literature analyzing lifetime of the PV inverter during the HCC operation mode, this master thesis intends to fill this void. Therefore, the main goals of this work are listed:

Goal 1: Lifetime evaluation considering the damage due to the environments disturbances (long-term analysis). Real mission profile of solar irradiance and ambient temperature are taking into account. Nevertheless, real mission profile of harmonic amplitude and phase angle are considered.

Goal 2: Lifetime evaluation considering the damage due to the power device switching frequency (short-term analysis). The mission profile of the environment conditions and harmonic parameters are also considered in this work.

1.3 Methodology

The methodologies to achieve these goals are:

- Mathematical modeling of the single-phase PV inverter connected to the electrical grid during HCC operation mode .
- Mathematical modeling of the switching and conduction power losses in the semiconductor devices considering the HCC operation mode.
- Simulation results in PLECS environment using computational model.
- Statistical analysis application in order to estimate the damage caused in the PV inverter during HCC.

1.4 Contributions

Considering the above discussions, the main contributions of this work are:

- Conduction and Switching power losses modeling for a semiconductor device considering the PV inverter in the HCC mode.
- For the first time, the long-term lifetime methodology is applied to the PV inverter during the HCC operation mode.
- Proposing a methodology to estimate the short-term lifetime consumption of a PV inverter during the HCC operation mode.

The results produced in this work originated two journal papers. The first one is already published and it is titled as:

R. C. de Barros, E. M. S. Brito, G. G. Rodrigues, V. F. Mendes, A. F. Cupertino, and H. A. Pereira, “Lifetime evaluation of a multifunctional pv single-phase inverter during harmonic current compensation,” in Microelectronics Reliability, September 2018, pp. 1071–1076.

The second paper was sent to IEEE Journal of Power Electronics with the follow tittle:

”Methodology for Short-Term Lifetime Evaluation of Multifunctional PV Inverter during Harmonic Current Compensation”.

1.5 Text Organization

This master thesis is outlined as follows:

Chapter 2 describes a single-phase PV system with HCC operation mode, focusing on the control strategy and the effect in the semiconductor device power losses due to the harmonic current component mitigation. In addition, the mathematical modeling for the conduction and switching power losses are proposed.

In chapter 3, the lifetime evaluation of the PV inverter considering the long-term time scale is presented. In addition, the conventional methodology to estimate the short-term lifetime consumption of a traditional PV inverter is also shown. In chapter 4, a proposed methodology to estimate the short-term lifetime consumption for a multifunctional PV inverter during the HCC operation mode is presented.

Chapter 5 presents a case study in order to exemplify the lifetime evaluation of a single-phase PV inverter with HCC operation mode. In chapter 6, based on mission profile real data of solar irradiance, ambient temperature, harmonic current components and phase angle, the lifetime consumption for long-term and short-term are presented. Finally, the conclusions are stated in chapter 7.

2 Single-Phase PV Inverter during HCC

In this chapter, an overview on the basic structure and functions of the single-phase PV system during HCC operation mode is described. In addition, the conduction and switching power losses modeling for the semiconductor power devices during the HCC process is performed.

2.1 Multifunctional PV Inverter and Control Strategy

The high penetration of distributed generation and the increasing of nonlinear loads connected to the power system make it more decentralized and vulnerable (TODESCHINI, 2017). Therefore, the PV system are expected to be more controllable and operate with high efficiency and reliability. A typical single-phase grid connected PV inverter with harmonic current compensation is presented in Figure 4.

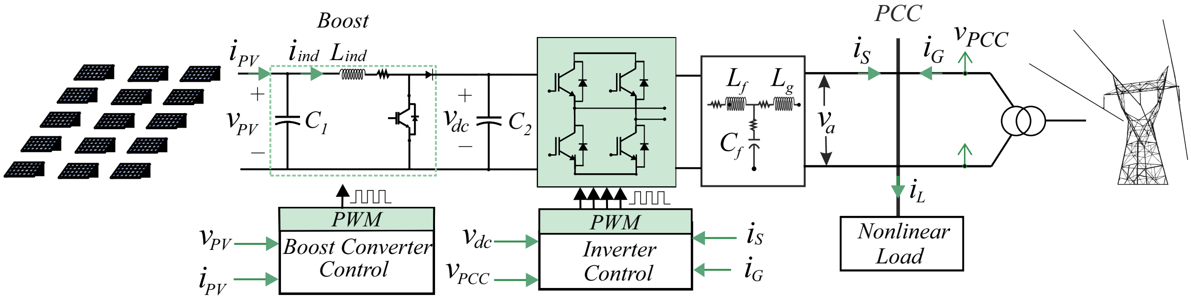

Figure 4 – Structure of a single-phase multifunctional PV inverter connected into the grid during the HCC operation mode.

Basically, the structure of the single-phase PV system is composed by two stages: dc/dc and dc/ac stages. The components of each stage and the control strategy are described in the next sections.In order to identify the harmonic components present in the nonlinear loads, a current sensor is necessary to detect the load current, mainly if the control strategy is performed by current controllers. For these purposes, the load current information is taken from the sum between the inverter and the grid current.

2.1.1 dc/dc Stage

This stage is composed by the PV panels and a boost converter. The PV panels generate active power converting the solar energy to electrical energy, which is injected into the electrical grid. The PV panels can be connected to each other in series or in parallel, depending of the amount of output current and voltage supported by the PV inverter.

The boost converter is essential to dc/dc stage for single-phase PV inverters, since there are power oscillation in the 2^{nd} harmonic frequency (BLAABJERG et al., 2006). This power oscillation causes dc-link voltage fluctuation, which is a negative factor considering the maximum power extraction from the PV array. Therefore, the boost converter is widely used to perform the the maximum power tracking (MPPT) algorithm (YANG K. ZHOU, 2015). In addition, this converter is responsible to guarantee the minimum voltage level at the dc-link in order to inject active power into the electrical grid during low solar irradiance conditions.

In this context, as shown in Figure 5, the boost block diagram is composed by a voltage loop. The output voltage v_{PV} and current i_{PV} from the PV array are used as input of the MPPT algorithm. Thus, the voltage reference v^{*}_{PV} is calculated and a PI control is used in order to send the pulse width modulation (PWM) signal to the semiconductor devices of the boost converter.

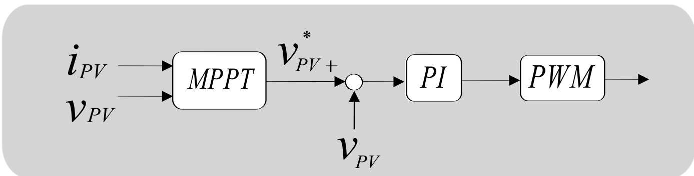

Figure 5 – The boost converter block diagram control.

2.1.2 dc/ac Stage

This stage is responsible to transform the direct to alternate current in order to inject the active power generated by the PV array into the electrical grid. The power flow is achieved by controlling the dc-link voltage. In addition, this stage is responsible to perform the ancillary services, such as the harmonic current compensation.

A LCL filter is connected to the PV inverter output. The filter is responsible to reduce the harmonic components generated by the converter switching. There are some filters topologies available in the literature, such as the L filters. They are an attractive solution due to their simple implementation. In the other hand, in practical operation, the use of LCL filters has a better cost-benefits ratio due to lower volume compared to L filters for similar attenuation capacity (GOMES A.F. CUPERTINO, 2018). In this work, a LCL filter is used in the single-phase PV inverter simulation. The design procedure for the LCL filter can be found in (P-ALZOLA et al., 2014).

The block diagram of the dc/ac stage is presented in Figure 6. Furthermore, the dc-link voltage is controlled by the outer loop. The fundamental current $i^{*}_{f}(t)$, which must be injected into the grid, is computed. Then, $i^{*}_{f}(t)$ is synchronized with the grid voltage, which is measured in the point of common coupling voltage , v_{PCC}. Moreover, the load harmonic current $i_h(t)$ is added to the $i_f^*(t)$ in order to generate the inverter reference current $i_s^*(t)$. Therefore, the inverter current $i_s(t)$ is controlled using a proportional multi-resonant controller (PMR) (XAVIER et al., 2015).

Both precision and control complexity are influenced by the controller. Proportional integral (PI) controllers have easier implementation. However, it presents steady state error due to their limited bandwidth. In this context, proportional resonant controllers (PR) have better precision (XAVIER et al., 2015). The resonant controller provides a theoretical infinite gain at the resonant frequency and reduces the steady state error. However, in the HCC operation mode, the PV inverter can compensate more than one harmonic order. Therefore, the PMR can be used in this application.

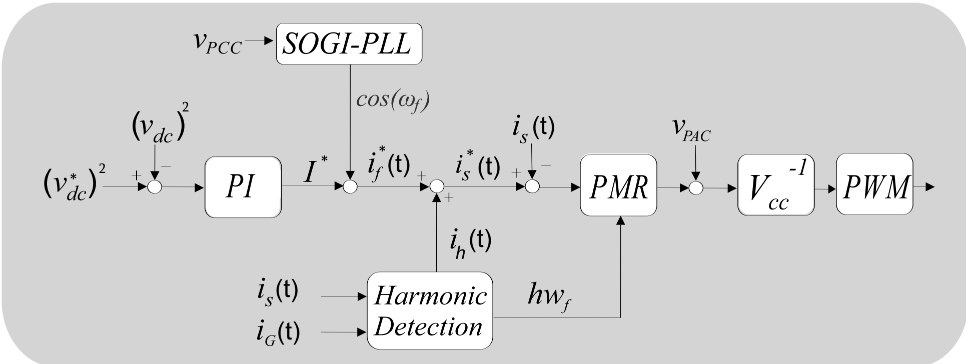

Figure 6 – PV inverter block diagram control.

2.1.3 Harmonic Detector Structure

In the HCC operation mode, the detection method of the nonlinear load harmonic current is an important issue. The current harmonic detector used in this work is based on the second-order-generalized-integrator (SOGI) structure connected in cascade with a synchronous phase-locked-loop (PLL) (CIOBOTARU; TEODORESCU; BLAABJERG, 2006). This technique takes advantages of the frequency adaptive characteristic of the SOGI structure, tuning in the frequency detected by the PLL. In addition, the harmonic detector used in this work is composed by two stages. The first one detects the amplitude of the fundamental current component $I_{f,d}$ and its frequency $\omega_{f,d}$. Afterward, $i_{f,d}(t)$ is subtracted from the load current $i_L(t)$ and the second stage detects the harmonic order h with higher current amplitude I_h. This is an interesting strategy because it can compensates harmonics with higher amplitude, reducing the total current harmonic distortion (THD). The structure of the harmonic detector is presented in Figure 7.

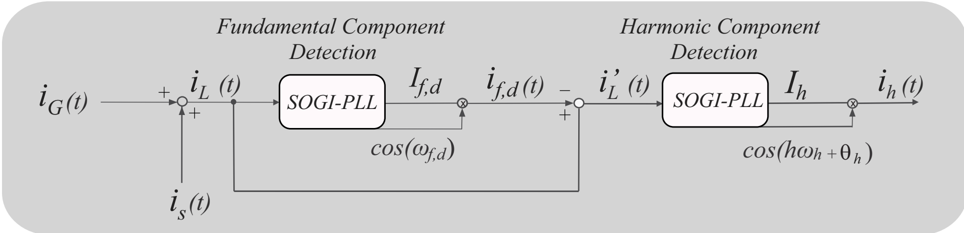

Figure 7 – Harmonic current detector based on the SOGI-PLL structure composed by two stages.

2.2 Effect of HCC operation mode in the Power Devices

Considering a PV inverter used to inject the harmonic components to supply the nonlinear load, the current through the power modules has different shapes depending on the harmonic component order, phase angle and harmonic amplitude. Therefore, in order to identify the power losses behavior in the semiconductor devices, it is necessary to identify the inverter current behavior. Considering the voltage at the point of common coupling is giving by:

$$V_{PCC} = V_g cos(\omega_f t), \tag{2.1}$$

where V_g is the peak grid voltage ($220\sqrt{2}\ V$) and ω_f represents the angular fundamental frequency equal to $2\pi 60\ rad/s$. The load current $i'_L(t)$ is composed by the sum of different harmonic orders k. In addition, each harmonic order can have current amplitude I_k and phase angle θ_k, as shown in the following equation:

$$i'_L(t) = \sum_{k=2}^{\infty} I_k sen(h\omega_f t + \theta_k). \tag{2.2}$$

As previously discussed, the harmonic current detected in the second stage of the harmonic detector structure is composed by the highest harmonic amplitude I_h with frequency $h\omega_f$ and phase angle θ_h, as showed in:

$$i_h(t) = I_h sen(h\omega_f t + \theta_h). \tag{2.3}$$

Since this inverter topology is expected to inject the fundamental current $i_f(t)$ and compensate the harmonic component with the highest amplitude, the reference of the inverter current is obtained by:

$$i_s^*(t) = I_f sen(\omega_f t) + I_h sen(h\omega_f t + \theta_h), \tag{2.4}$$

where I_f is the fundamental current generated by the PV panels.

Therefore, the current signal generated by the PV inverter depends on the harmonic component parameters (h, I_h, and θ_h). In order to illustrate this fact, the current signal of a PV inverter compensating 3^{rd}, 5^{th} and 7^{th} harmonic orders with phase angle 0° and 180° are shown in Figure 8. As noticed, depending on the θ_h value, the emergence of local maximum and minimum appear in the inverter current. Since the conduction power loss depends on the current shape, it is expected that h, I_h and θ_h values directly affect the conduction and switching power losses.

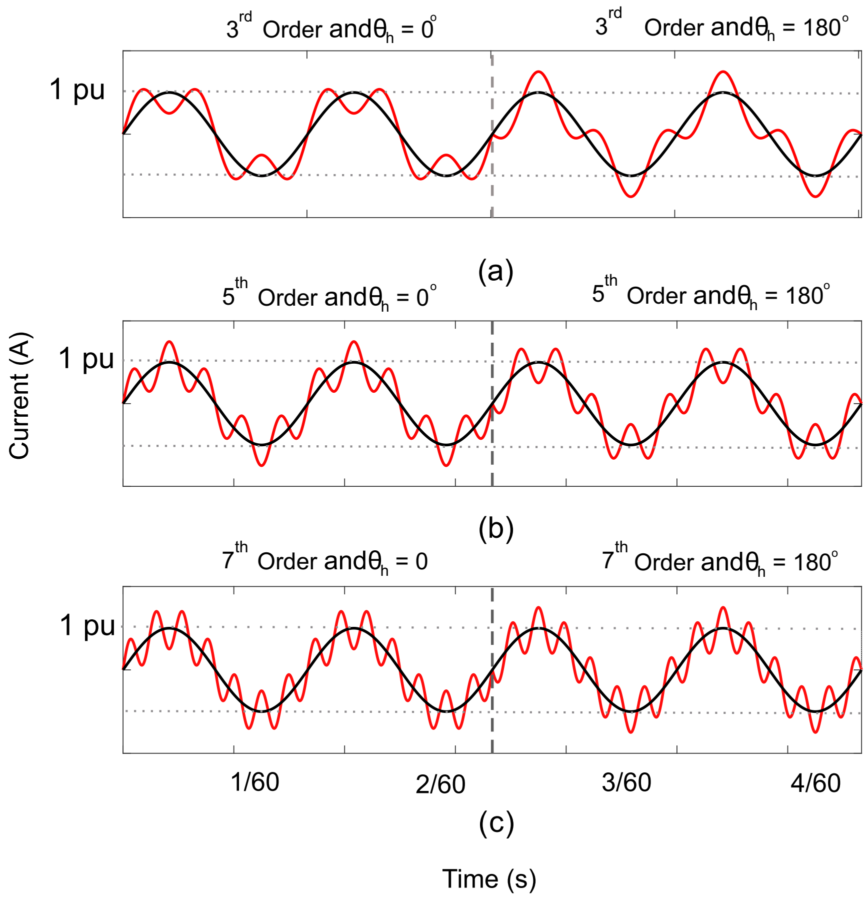

Figure 8 – Current shape of the PV inverter injecting the nominal active power (5 kW) and compensating 0.3 pu of: (a) 3^{rd} harmonic current component with phase angle 0° or 180°, (b) 5^{th} harmonic current component with phase angle 0° or 180° and (c) 7^{th} harmonic current component with phase angle 0° or 180°.

2.3 IGBT Power Losses Modeling During the HCC Operation Mode

Considering the reliability analysis of the semiconductor power devices, it is important to understand their power losses behavior. The semiconductor power losses can be calculated by establishing physical models or considering mathematical calculation methods. Physical models were used in previous works (REIGOSA, 2014), (BRITO et al., 2018), since it is possible to use the component parameters given by manufacturer datasheets (WEI et al., 2017). However, depending on the manufacturer, the information is difficult to be obtained or it is not provided. In addition, the simulation speed using those model is very low and time consuming.

Previous studies have performed mathematical equations to estimate the power losses in a IGBT for a traditional PV inverter operation (FEIX et al., 2009) (CHEN; STUART, 1992). However, there is no work in the literature proposing mathematical models to calculate the power losses during the HCC operation mode. Therefore, this work aims to fill this void proposing analytical equations to estimate the IGBT power losses considering the HCC operation mode.

Basically, there are two types of power losses in a semiconductor device: the conduction and switching power losses. The conduction losses occur when the semiconductor device is in full conduction. The current in the component is whatever is required by the circuit and the voltage at its terminals is the voltage drop due to the device itself. The switching losses, occurs when the device is transitioning from the blocking state to the conducting state and vice-versa (FEIX et al., 2009). The curves considering the IGBT collector current i_c and the voltage collector-emitter v_{ce} during the conduction and switching stages are shown in Figure 9. In this context, the conduction and switching power losses modeling are discussed in the following sections.

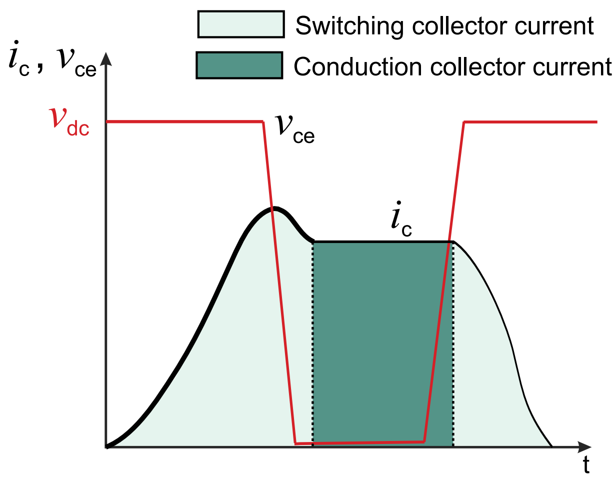

Figure 9 – v_{ce} and i_c IGBT curves during the conduction and switching process.

2.3.1 Conduction Power Losses

The conduction power losses is directly related to the conducting voltage v_{ce} and forward current i_c behaviors. Those information are obtained from the IGBT manufacture datasheet and they are presented for a specific junction temperature, T_j. For the datasheet used in this work, which part number is IKW20N60T, the v_{ce} and i_c curves are provided for T_j equal to 25 °C and 175 °C . However, in this work, the junction temperature was designed to be set at 100 °C during the PV inverter nominal operation. Therefore, a curve for T_j equal to 100 °C was estimated by linear interpolation, based on the curves from 25 °C and 175 °C temperatures, as shown in Figure 10(a).

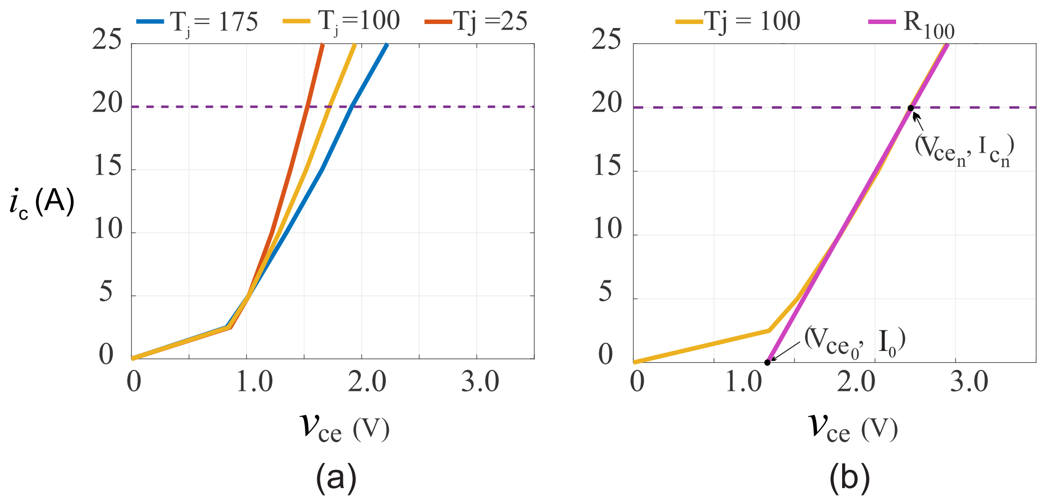

Figure 10 – v_{ce} and i_c IGBT curves representation: (a) the curves for T_j equal to 25 °C, 175 °C and the estimated curve for T_j equal to 100 °C, (b) equation line approximation for v_{ce} and i_c considering (V_{cen}, I_{cn}) and (V_{ce_0},I_0).

According to (BARBI, 2008), the curve of v_{ce} and i_c can be approximated to a line equation R_{100} in order to simplify the conduction losses calculation, as shown in Figure (10)(b). Thus, two points of (v_{ce},i_c) are considered. One of them is the nominal operation point, which is (V_{cen}, I_{cn}) and the second point (V_{ce_0}, I_0) is chosen in order to have the best fit of the original curve considering the collector current equal to zero. Therefore, R_{100} can be found by:

$$R_{100} = v_{ce} = \left(\frac{V_{cen} - V_{ce_0}}{I_{cn}}\right) i_c + V_{ce_0}. \tag{2.5}$$

The current which flows though the IGBT can be estimated by the PV inverter output current i_s. Since the inverter used in this work is a single-phase PV system compensating harmonic current components, the output current is represented by:

$$i_s = I_f sen(\omega_f t) + I_h sen(h\omega_f t + \theta_h). \tag{2.6}$$

Since the nonlinear inverter is connected in parallel to the grid, the inverter output voltage v_a is equal to the grid voltage. Thus, the harmonic voltage components are not considered in this work, as presented in the following equation:

$$v_a = V_g sen(\omega_f t). \tag{2.7}$$

The current which flows in the IGBT is directly related to the duty cycle δ (FEIX et al., 2009). Because the modulation technique used in this work is the PWM, as showed in Figure 11, the duty cycle can be calculated according to (BARBI, 2008), as shown in the following equation:

$$\delta = \frac{t_s}{T_s} = \frac{v_a + v_{dc}}{2v_{dc}} = \frac{1}{2}\left[1 + msen(\omega_f t)\right], \tag{2.8}$$

where m is the modulation index equal to $\frac{V_g}{v_{dc}}$ and t_s is the time which the IGBT is turned on during a time period T_s of the carrier wave. Therefore, the inverter current can be obtained by:

$$i_c = i_a\delta = \frac{1}{2}\left[I_f sen(\omega_f t) + I_h sen(h\omega_f t + \theta_h)\right]\left[1 + msen(\omega_f t)\right]. \tag{2.9}$$

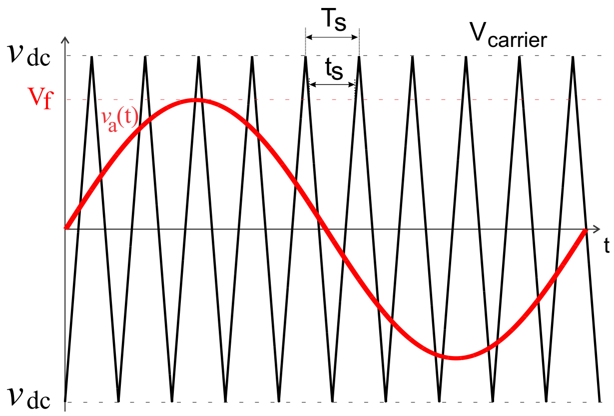

Figure 11 – PWM modulation considering the carrier wave with period T_s and the signal modulation.

Replacing $\omega_f t$ for a variable α, i_c is represented as:

$$i_c(\alpha) = \frac{1}{2}\left[I_f sen(\alpha) + I_h sen(h\alpha + \theta_h)\right]\left[1 + msen(\alpha)\right]. \tag{2.10}$$

The conduction power losses is estimated using the instantaneous energy $E_{i,cond}(\alpha)$ dissipated in the IGBT considering the period of time equal to δTs, as shown in:

$$E_{i,cond}(\alpha) = v_{ce}(\alpha) i_c(\alpha) \delta(\alpha) T_s. \tag{2.11}$$

Applying (2.5),(2.8),(2.10) to (2.11), the instantaneous energy can be written considering the parameters of the PV inverter compensating harmonic current component. Since the switching frequency f_s is larger than the fundamental frequency, it is possible to condenser (2.11) as a differential equation, as proposed by (BARBI, 2008) and presented in the following equation:

$$\frac{E_{i,cond}(\alpha)}{dt} = v_{ce}(\alpha) i_c(\alpha) \delta(\alpha). \tag{2.12}$$

Thus, the instantaneous power losses $P_{i,cond}$ can be estimated by using the concept of average power, as shown in:

$$P_{i,cond}(\alpha) = \frac{E_{i,cond}(\alpha)}{dt}. \tag{2.13}$$

Therefore, considerinng $dt = d\alpha/w$ e $w = 2\pi/T$, the average conduction power losses P_{cond} can be calculated by:

$$P_{cond} = \frac{1}{T}\int_0^T P_{i,cond}(\alpha) dt. \tag{2.14}$$

Since the solution for equation (2.14) is larger and time consuming, the result for a specific harmonic order is shown in (2.15). In this case, the third harmonic order is chosen.

$$P_{cond} = [m(105\pi + 420) + 280mI_f^2 + I_h^2\left(\frac{V_{cen} - V_{ce_0}}{I_{cn}}\right)\pi(105\pi + 240m) + cos(\theta)(140I_h + 12mI_h^2)\left(\frac{V_{cen} - V_{ce_0}}{I_{cn}}\right)cos(\theta_h) - \left(\frac{V_{cen} - V_{ce_0}}{I_{cn}}\right)112mI_hI_f]\left(\frac{1}{140\pi}\right). \tag{2.15}$$

2.3.2 Switching Power Losses

The switching power losses are divided in two stages: the turn-on and turn-off stage. Thus, for each stages, analytical equations for the switching losses are proposed in the following sections.

When the IGBT is in the turn-on stage, the characteristic curve of v_{ce} and i_c are shown in Figure 12(a). In order to make easier the instantaneous energy $E_{i,on}$ calculation, the curve i_c is approximated to a linear curve as shown in Figure 12(b). Thus, the $E_{i,on}$ can be estimated considering the energy in the area A, B and C of the linear curve approximation.

For the area A, the instantaneous energy $E_{i,A,on}$ are estimated by:

$$E_{i,A,on}(\alpha) = \int_0^{t_r} v_{ce} i_c(\alpha) dt = v_{dc}\int_0^{t_r} i_c(\alpha) dt = v_{dc}\frac{i_c(\alpha) t_r}{2}. \tag{2.16}$$

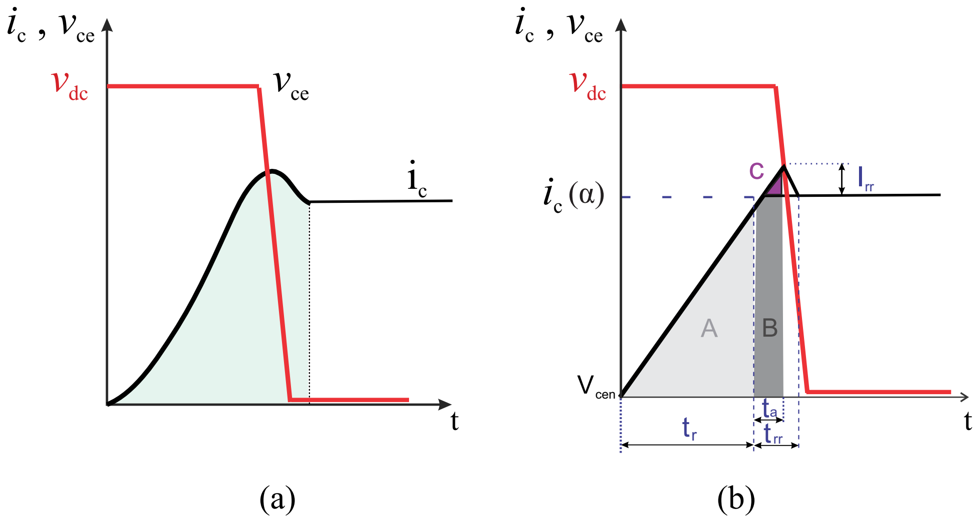

Figure 12 – Characteristic curve of the IGBT during the turn-on stage. In (a), the real curves of v_{ce} and ic are presented. In (b), the approximated curves are shown.

where t_r is the rising time. According to (CHEN; STUART, 1992), the rising time can be estimated using the parameters obtained from the datasheet, as shown in the following equation:

$$t_r = \frac{t_{rn}}{I_{cn}} i_c(\alpha), \tag{2.17}$$

where t_{rn} is the nominal rising time of the inverter current. I_{cn} is the nominal collector current when $t = t_{rn}$. Applying (2.17) to (2.16), the instantaneous energy in the area A $E_{i,A,on}$ is represented in (2.18).

$$E_{i,A,on} = v_{dc} \frac{t_{rn}}{2} \frac{i_c^2(\alpha)}{I_{cn}}. \tag{2.18}$$

The i_c behavior in the area B and C have the influence of the diode connected in parallel with the IGBT. Thus, the parameters of I_{rr} and t_{rr}, which are shown in Figure 12, are calculated in (2.19) and (2.20), as proposed by (KOLAR; ZACH; CASANELLAS, 1995).

$$I_{rr} = \left(0.7 + \frac{0.3 i_c(\alpha)}{I_{cn}}\right) I_{rrn}, \tag{2.19}$$

$$t_{rr} = \left(0.8 + \frac{0.2 i_c(\alpha)}{I_{cn}}\right) t_{rrn}, \tag{2.20}$$

where the values of nominal reverse current of diode I_{rrn} and nominal reverse time t_{rrn} are found in the datasheet.

The energy in the area B, $E_{i,B,on}$, can be estimated as:

$$E_{i,B,on}(\alpha) = \int_0^{t_a} v_{ce} i_c(\alpha) dt = v_{dc} \int_0^{t_a} i_c(\alpha) dt = v_{dc} i_c(\alpha) t_a. \tag{2.21}$$

Therefore, considering the approximation t_{rr} is equal to t_a, as proposed by (KOLAR; ZACH; CASANELLAS, 1995), the instantaneous energy $E_{i,B,on}$ can be estimated as:

$$E_{i,B,on}(\alpha) = v_{dc} i_c(\alpha) t_{rr}. \tag{2.22}$$

Thus, applying (2.20) to (2.22), the $E_{i,B,on}$ can be estimated as:

$$E_{i,B,on}(\alpha) = v_{dc} i_c(\alpha) \left(0.8 + \frac{0.2 i_c(\alpha)}{I_{cn}} \right) t_{rrn}. \tag{2.23}$$

The energy in the area C $E_{i,C,on}$ is calculated according with the following equation:

$$E_{i,C,on}(\alpha) = \int_0^{t_a} v_{ce} i_c(\alpha) dt = v_{dc} \int_0^{t_a} i_c(\alpha) dt = v_{dc} \frac{I_{rr} t_a}{2}. \tag{2.24}$$

Thus, using the same approximation ($t_a \approx t_r$) and applying the equation (2.19) and (2.20) in (2.24), the $E_{i,C,on}$ is estimated as:

$$E_{i,C,on}(\alpha) = v_{dc} \frac{\left(0.7 + \frac{0.3 i_c(\alpha)}{I_{cn}}\right) I_{rrn} \left(0.8 + \frac{0.2 i_c(\alpha)}{I_{cn}}\right) t_{rrn}}{2}, \tag{2.25}$$

$$E_{i,C,on}(\alpha) = v_{dc} \left(0.28 + 0,19 \frac{i_c(\alpha)}{I_{cn}} + 0.03 \left(\frac{i_c(\alpha)}{I_{cn}} \right)^2 \right) Q_{rrn}, \tag{2.26}$$

where Q_{rrn} is the nominal diode reverse recovery charge, which is equal to $t_{rrn} I_{rrn}$.

Thus, the total instantaneous energy during the IGBT turn-on stage for the area A, B and C is described in the following equation:

$$E_{i,sw,on}(\alpha) = E_{i,A,on}(\alpha) + E_{i,B,on}(\alpha) + E_{i,C,on}(\alpha). \tag{2.27}$$

Considering the switching frequency higher than the grid frequency, the instantaneous power losses in the turn on stage $P_{i,sw,on}$ can be estimated as:

$$P_{i,sw,on}(\alpha) = \frac{E_{i,sw,on}(\alpha)}{dt} = \frac{E_{i,sw,on}(\alpha)}{T_s} = \frac{d(E_{A,on}(\alpha) + E_{B,on}(\alpha) + E_{C,on}(\alpha))}{T_s}. \tag{2.28}$$

Thus, considering the manipulation $dt = d\alpha/w$ e $w = 2\pi/T$, the average power losses in the turn on stage $P_{sw,on}$ can be calculated as:

$$P_{sw,on} = \frac{1}{T}\int_0^T P_{i,sw,on}. \tag{2.29}$$

Thus, integrating the instantaneous power losses in a half cycle of the grid frequency and applying the equation (2.27) in the (2.29), the $P_{sw,on}$ is estimated as:

$$P_{i,sw,on} = \frac{f_s}{2\pi}\int_0^\pi E_{i,A,on} d\alpha + \frac{f_s}{2\pi}\int_0^\pi E_{i,B,on} d\alpha + \frac{f_s}{2\pi}\int_0^\pi E_{i,C,on} d\alpha. \tag{2.30}$$

In order to reduce the integral calculation process, the $P_{sw,on}$ is calculated for an specific harmonic order. In this case, the third harmonic order is chosen and the result is presented in the following equation:

$$\begin{aligned} P_{sw,on} = {} & \frac{v_{dc}t_{rrn}\left(\pi I_f^2 + 16 I_{cn} I_f + \pi I_h^2\right)}{10 I_{cn}} + \frac{\left(v_{dc} f_s t_{rrn}\left(I_f^2 + I_h^2\right)\right)}{8 I_{fn}} + \\ & \frac{\left(v_{dc} f_s t_{rrn}\left(3\pi I f^2 + 48 I_{fn} I f + 3\pi I_h^2 + 16 I_{cn} cos(\theta_h) I_h\right)\right)}{60 I_h \pi} + \\ & \frac{\left(Q_{rrn} v_{dc} f_s\left(168\pi I_{cn}^2 + 228 I_{cn} I_f + 76 cos(\theta_h) I_{cn} I_h + 9\pi I_f^2\right)\right)}{1200 I_{cn}^2 \pi}. \end{aligned} \tag{2.31}$$

The typical i_c and v_{ce} curves when the IGBT is turned off are shown in Figure 13(a). In order to facilitate the instantiations $E_{i,off}(\alpha)$ estimation during the turn-off stage, an area approximation A' was proposed by (BARBI, 2008), as presented in Figure 13(a).

Using the same idea of the area calculation in the previous section, the instantiations $E_{i,off}(\alpha)$ can be represented in by:

$$E_{i,off}(\alpha) = \int_0^{t_f} v_{ce} i_c(\alpha) dt = v_{dc}\int_0^{t_f} i_c(\alpha) dt = v_{dc}\frac{i_c(\alpha) t_f}{2}. \tag{2.32}$$

According to (KOLAR; ZACH; CASANELLAS, 1995), the falling time t_f of the inverter current can be estimated as:

$$t_f = \left(\frac{2}{3} + \frac{i_c}{3 I_{cn}}\right) t_{fn}, \tag{2.33}$$

where t_{fn} is the falling time of the nominal inverter current, which is provided by the manufactures.

Thus applying (2.33) in (2.32), the E_{off} (α) can be expressed as:

$$E_{i,off}(\alpha) = \frac{v_{dc} i_c(\alpha)\left(\frac{2}{3} + \frac{i_c}{3 I_{cn}}\right) t_{fn}}{2}. \tag{2.34}$$

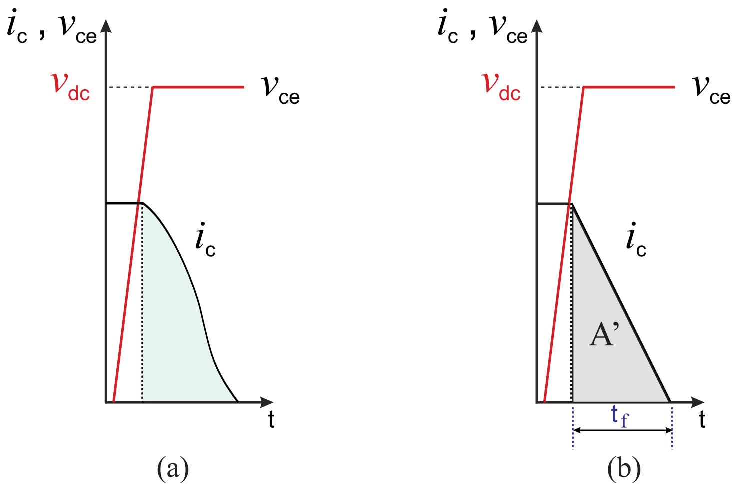

Figure 13 – Characteristic curve of the IGBT during the turn-off stage. In (a), the real curves of v_{ce} and ic are presented. In (b), the approximated curves are shown.

Considering the switching frequency higher than the grid frequency, the instantaneous power losses in the turn off stage $P_{i,off}$ can be estimated as:

$$P_{i,off}(\alpha) = \frac{d(E_{i,off}(\alpha))}{dt} = \frac{E_{i,off}(\alpha)}{T_s} = \frac{\frac{1}{2}v_{dc}i_c(\alpha)\left(\frac{2}{3}+\frac{i_c}{3I_{cn}}\right)t_{fn}}{T_s}. \tag{2.35}$$

Thus, considering the manipulation $dt = d\alpha/w$ e $w = 2\pi/T$, the average power losses in the turn on stage $P_{sw,off}$ can be calculated as:

$$P_{sw,off} = \frac{1}{T}\int_0^T P_{i,off}. \tag{2.36}$$

Thus, integrating the instantaneous power losses in a half cycle of the grid frequency and applying (2.35) in (2.36), the $P_{sw,off}$ is estimated as:

$$P_{sw,off} = \frac{f_s}{2\pi}\int_0^\pi E_{off}d\alpha = \frac{f_s}{2\pi}\int_0^\pi \frac{\frac{1}{2}v_{dc}i_c(\alpha)\left(\frac{2}{3}+\frac{i_c}{3I_{cn}}\right)t_{fn}}{T_s}d\alpha. \tag{2.37}$$

Therefore, for a specific harmonic order of the 3^{rd} harmonic component, the $P_{sw,off}$ is shown in:

$$P_{sw,off} = \frac{\left[v_{dc}f_st_{fn}\left(6\pi I_f^2 + 48I_{fn}I_f + 6\pi I_h^2 + 16I_hI_{cn}cos(\theta_h)\right)\right]}{(144I_{cn}\pi)}. \tag{2.38}$$

Finally, the total switching power P_{sw} losses are the sum of $P_{sw,on}$ and $P_{sw,off}$, as shown in (2.39).

$$P_{sw} = P_{sw,on} + P_{sw,off}. \tag{2.39}$$

Finally, replacing (2.31) and (2.38) to (2.39), the P_{sw} is estimated as:

$$
\begin{aligned}
P_{sw,off} = &\frac{v_{dc}t_{rrn}\left(\pi I_f^2 + 16I_{cn}I_f + \pi I_h^2\right)}{10I_{cn}} + \frac{\left(v_{dc}f_st_{rrn}\left(I_f^2 + I_h^2\right)\right)}{8I_{fn}} + \\
&\frac{\left(v_{dc}f_st_{rrn}\left(3\pi If^2 + 48I_{cn}If + 3\pi I_h^2 + 16I_{cn}cos(\theta_h)I_h\right)\right)}{60I_h\pi} + \\
&\frac{\left(Q_{rrn}v_{dc}f_s\left(168\pi I_{cn}^2 + 228I_{cn}I_f + 76cos(\theta_h)I_{cn}I_h + 9\pi I_f^2\right)\right)}{1200I_{cn}^2\pi} + \\
&\frac{\left[v_{dc}f_st_{fn}\left(6\pi I_f^2 + 48I_{fn}I_f + 6\pi I_h^2 + 16I_hI_{cn}cos(\theta_h)\right)\right]}{(144I_{cn}\pi)}.
\end{aligned} \tag{2.40}
$$

Performing a simulation on PLECs, the average of the conduction and switching power losses are compared to those values obtained from the model in (2.40) and (2.38), respectively. Thus, a single phase PV inverter injecting the nominal active power of 5 kW is used. Considering the fundamental current I_f constant and equal to the nominal PV inverter current, the harmonic amplitude are varied from 0 A to the value of I_f. Also, the harmonic phase angle were varied from 0° to 360°. This procedure are made to the 3^{rd}, 5^{th} and 7^{rd} harmonic orders. The estimated conduction and switching power losses from PLECs and the model are shown in Figure 14 and Figure 15, respectively. In addition, the parameters used from the datasheet are described in Table 1.

Table 1 – IGBT parameters from the datasheet necessary to calculate the conduction power losses.

Parameter	Lable	Value
IGBT collector-emitter voltage in nominal operation	V_{cen}	2.35 V
IGBT on-state zero current collector-emitter voltage	V_{ce_0}	1.7 V
dc-link voltage	v_{dc}	390 V
IGBT collector current in nominal operation	I_{cn}	20 A
Diode reverse recovery charge	Q_{rr}	0.31 μC
Fundamental current amplitude	I_f	16 A
Harmonic current amplitude	I_h	from 0 A to 16 A
Harmonic phase angle	θ_h	from 0° to 360°

As noticed in Figure 14 and Figure 15, the power losses estimated by the model present differences comparing to the power losses values from PLECs. For all the harmonic order, the relative error does not achieve 4 % for the conduction losses and 6 % for the switching losses. The error increases with the increasing of the harmonic amplitude. Also, the error is more significant for phase angle equal to 180°.

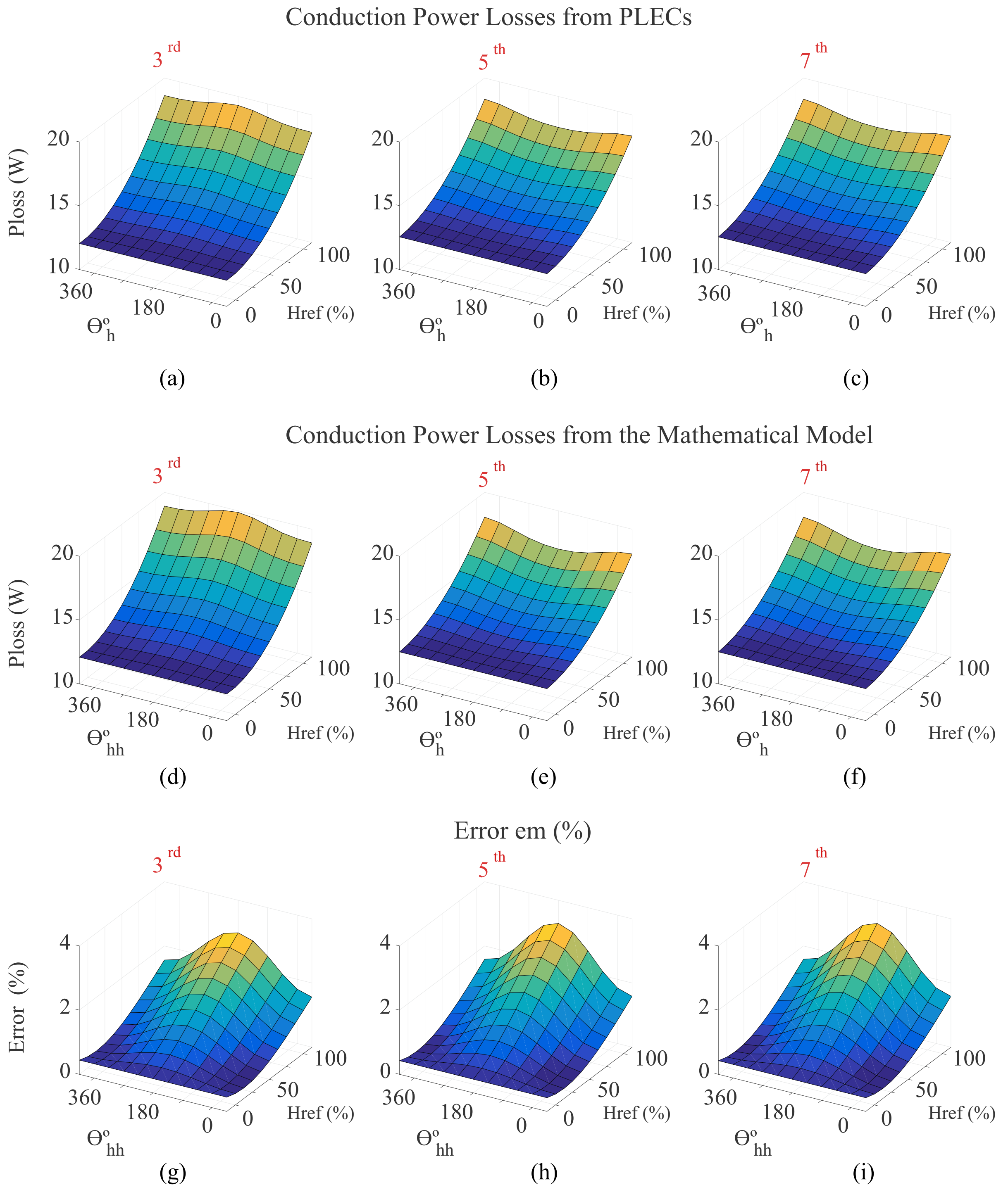

Figure 14 – Conduction power losses from PLECs considering the: (a) the 3^{rd}, (b) 5^{th} and (c) 7^{th} harmonic component. In addition, the conduction power losses for the analytical model (d) the 3^{rd}, (e) 5^{th} and (f) 7^{th}. The relative error is also presented for (g) 3^{rd}, (h) 5^{th} and (i) 7^{th}.

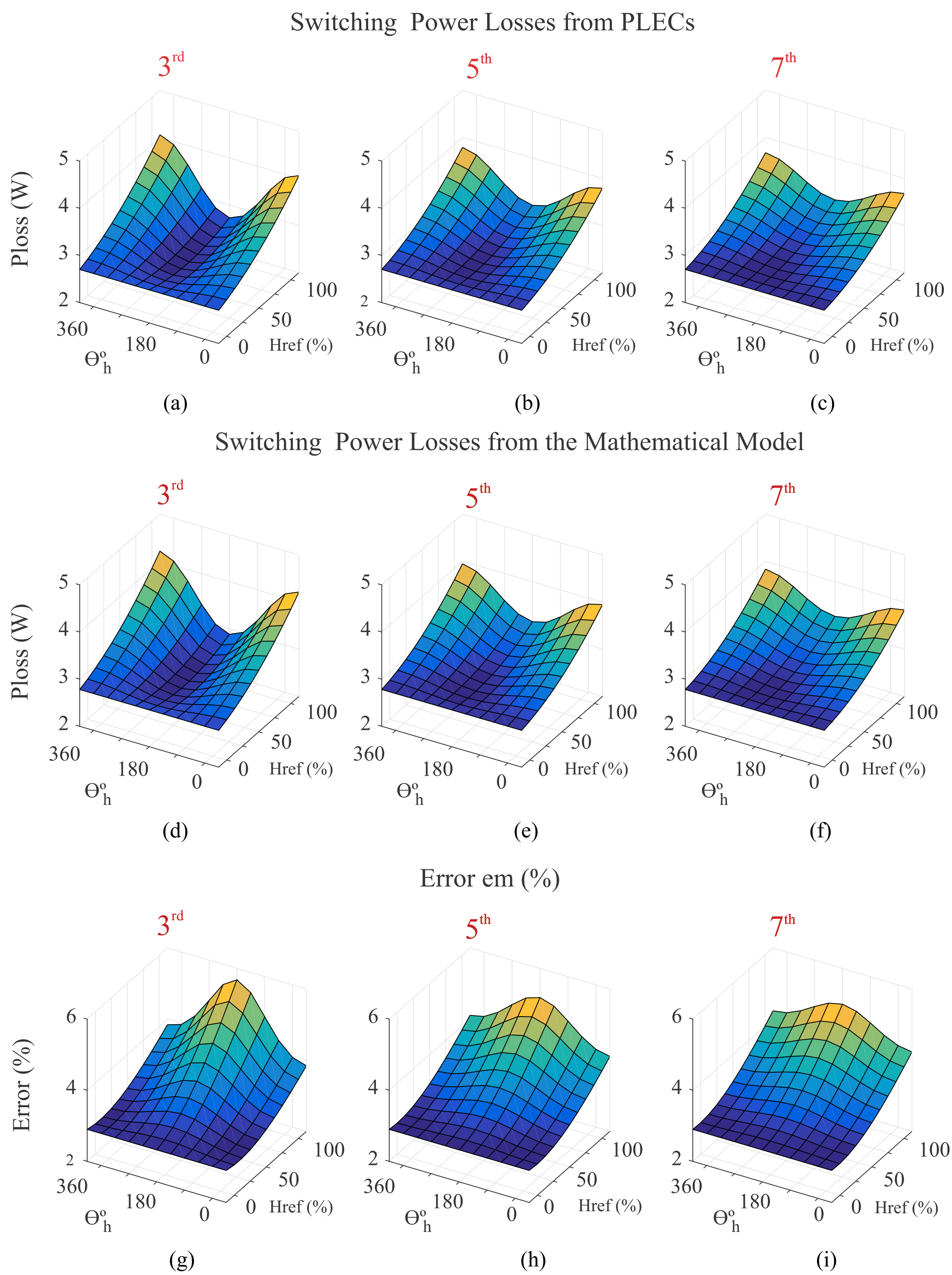

Figure 15 – Switching power losses form PLECs considering the: (a) the 3^{rd}, (b) 5^{th} and (c) 7^{th} harmonic component. In addiction, the conduction power losses for the analytical model (d) the 3^{rd}, (e) 5^{th} and (f) 7^{th}.The relative error is also presented for (g) 3^{rd}, (h) 5^{th} and (i) 7^{th}.

3 Reliability Evaluation During Harmonic Current Compensation

In this chapter, the methodology to estimate the PV inverter lifetime consumption is provided. Previous studies have demonstrated that mission profiles highly affect the semiconductor reliability (MA et al., 2015; SANGWONGWANICH et al., 2018). This consideration may involve multidisciplinary models with quite different time constants, which are related to the power cycling over the semiconductor device (REIGOSA et al., 2016). Thus, two time constants will be considered in this work: the long-term and short-term. The lifetime consumption for each of them is described in the following sections. In addition, with the methodology available in the literature, the long-term lifetime evaluation during the HCC operation mode can be evaluated. On the other hand, there is a gap in the literature regarding the short-term lifetime evaluation, since there are additional power cycles due to the harmonic current components.

3.1 Long-Term Lifetime Estimation

Previous works have concluded that junction temperature T_j, fluctuation junction temperature ΔT_j and the heating time t_{on} directly affect the semiconductor lifetime consumption (SANGWONGWANICH et al., 2018), (REIGOSA et al., 2016). Since these variables change with the mission profile, the long-term analysis intends to quantify the damage in the semiconductor device due to the power cycling caused by the environmental variation.

Thus, it is necessary to estimate the values of T_j, ΔT_j and t_{on} considering the variation of the environmental conditions. In this way, an interesting solution is to use the power losses of the semiconductor device in order to estimate the junction temperature. It is possible because the power losses dissipated in the semiconductor device can be translated into an electrical thermal model, which is able to extract the T_j using a thermal circuit. Thus, from the junction temperature values, the ΔT_j and t_{on} can be estimated. The flowchart for the long-term lifetime evaluation is presented in Figure 17. Each step of this process is described in the following sections.

3.1.1 Thermal Loading and Rainflow Counting Algorithm

The first step is getting a mission profile of solar irradiance and ambient temperature from a specific region. Thus, the active power P_{out} generated by the PV panels can be

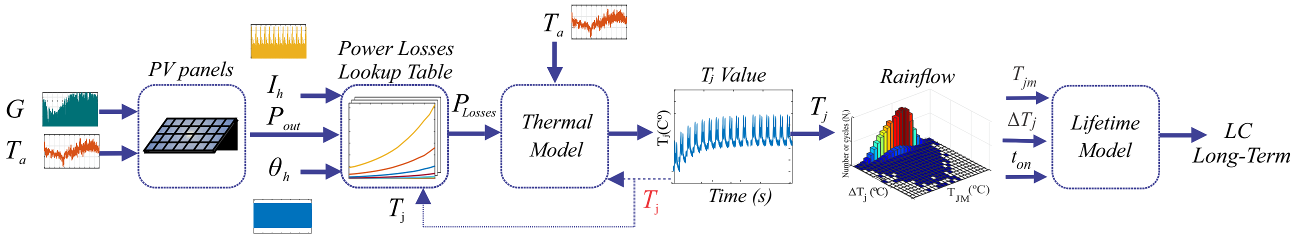

Figure 16 – Flowchart of the lifetime consumption calculation considering the long-term time scale.

estimated. In this work, P_{out} is estimated based on the reference (Villalva; Gazoli; Filho, 2009), which provides a simulation approach to estimate the output power from the photovoltaic arrays.

As shown in the chapter 2, the conduction and switching power losses depend on the harmonic order, phase angle, and current harmonic amplitude. Thus, a mission profile from a nonlinear load, considering the harmonic current components information, needs to be taken into account.

The basic idea is to create a power loss lookup table. Thus, for each specific point of the mission profile, the semiconductor device power losses can be estimated. In order to create the lookup table, the values of P_{out}, I_h, θ_h and T_j are varied in a simulation environment (PLECs) considering different combinations. Thus, for each combination of the mission profile, the semiconductor power losses are stored in a lookup table, as shown in Figure 17. It is important to observe that the power loss lookup table is created for a specific harmonic order.

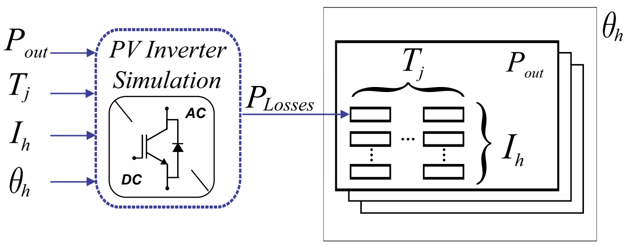

Figure 17 – Generation process of the power loss lookup table for a specific harmonic order.

The power losses are translated into an electrical thermal model, which is responsible for extracting the T_j. One of the most used thermal circuit is proposed by (MA et al., 2015), as shown in Figure 18. The $R_{eq(j-c)}$ represents the junction to case thermal resistance, $R_{eq(c-h)}$ the case to heat sink and $R_{eq(h-a)}$ the heat sink to ambient thermal resistance. In addiction, the thermal capacitance is represented by $C_{n(j-c)}$. This approach is composed by the advantages of Foster and Cauer thermal impedance model, achieving more accurate in the T_j and case temperature T_c estimation. The values of the thermal resistances $R_{eq(j-c)}$,

$R_{eq(c-h)}$ and thermal capacitance are provided by the manufacture datasheet.

The $R_{eq(h-a)}$ is not provided by the manufacture datasheet and its needed to be designed. Thus, a simplest solution is to use the electrical circuit information from Figure 18 . In this design methodology, only the steady-state is considered. Thus, the maximum heat sink temperature value T_{h_m} can be estimated as:

$$T_{h_m} = T_a + \left(R_{eq(h-a)}\right) P_{loss}. \tag{3.1}$$

Thus, the $R_{eq(h-a)}$ can be estimated as:

$$R_{eq(h-a)} = \frac{(T_{h_m} - T_a)}{P_{loss}}. \tag{3.2}$$

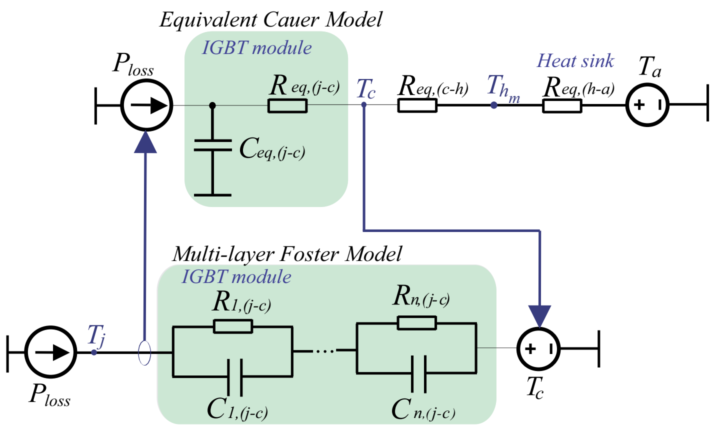

Figure 18 – Electrical thermal model based on Foster and Cauer model used for a single semiconductor device.

Since the junction temperature are estimated, it is used a rainflow counting algorithm in order to convert the randomly thermal profile into regulated thermal cycle, which is needed to compute the lifetime consumption. Rainflow counting has become the most widely accepted method for the processing of random signals for fatigue analysis, and tests have demonstrated good agreement with measured fatigue lives when compared to other counting algorithms (MARSH; WIGNALL; THIES, 2015). In addition, based on the T_j values, the rainflow is able to estimate the ΔT_j and the t_{on}.

3.2 Lifetime Model

With the values of T_j, ΔT_j and t_{on}, it is important to chose the lifetime model to estimate the lifetime consumption (LC) of the semiconductor device. In this context, there are empirical lifetime models proposed in the literature in order to estimate the number of cycles to failure N_f (HELD et al., 1997). In this work, the Bayerer model is used.

The Bayerer model is a lifetime estimation method proposed by (BAYERER et al., 2008). This model estimates the number of cycles until failure N_f of the power devices based on the T_j, ΔT_j and t_{on} values, as showed in (3.3). The parameters meaning and their limit considerations proposed by the Bayerer model are presented in Table 2 and they are discussed with more details in (BAYERER et al., 2008). It is important to observe that (3.3) takes into account the damage due the bond wire fatigue, considering a semiconductor device from Infineon.

$$N_f = A\,(\Delta T_j)^{\beta 1}\,exp\left(\frac{\beta_2}{T_j + 273}\right) t_{on}^{\beta 3} I^{\beta_4} V^{\beta 5} D^{\beta_6}. \tag{3.3}$$

Miner's rule, proposed by (HUANG; MAWBY, 2013), assumes that the damage accumulates linearly. Thus, it is commonly applied in order to calculate the accumulated fatigue damage. Thus, the N_f is calculated, the lifetime consumption LC over determinated mission profile is estimated using the Palmgren-Miner's rule, as showed in (3.4).

$$LC = \sum \frac{n_i}{N_f}, \tag{3.4}$$

where the number of cycles for a specific combination of T_j, ΔT_j and t_{on} is referred to as n_i.

Table 2 – Parameters and limits for N_F calculation based on the Bayerer model.

Parameter	Limits	Coef.	Value
Technology factor A	-	-	9.3410^{14}
Temp. fluctuation ΔT_j	45-150 $°C$	β_1	-4.416
Min. junction temp. T_{jm}	20-120 $°C$	β_2	1285
Cycling period t_{on}	1-60s	β_3	-0.463
Current per bond foot I	3-23A	β_4	-0.716
Blocking voltage/100 V	6-33V	β_5	-0.761
Bond wire diameter D	75-500μm	β_6	-0.5

3.3 Short-Term Lifetime Evaluation

The power cycling due to the line frequency strongly affects the lifetime consumption (BRITO et al., 2018), (REIGOSA et al., 2016). Thus, the short-term lifetime analysis intends to quantify the damage caused in the semiconductor device in a period T, equal to $1/f_o$, where f_o is the grid frequency. In order to illustrate the junction temperature behavior during this period, Figure 19 presents the T_j values of the semiconductor device for two different values of active power injected by the inverter. For this case, the PV inverter is only injecting the fundamental current, without the multifunctional operation. In this context, the values of T_j, ΔT_j and t_{on} needs to be estimated in order to evaluate the lifetime consumption.

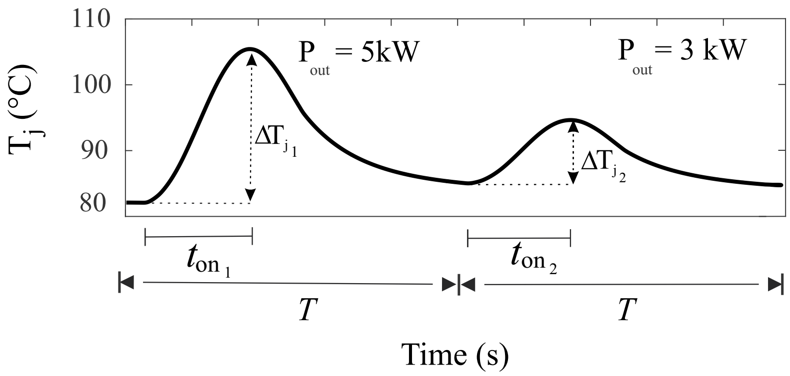

Figure 19 – Junction temperature behavior during the short-term analysis.

It is observed that the mission profile is hard to be obtained, since the sample frequency of data acquisition needs to be considerable high. Therefore, there are some methodology proposed in the literature in order to estimate the parameters of T_j, ΔT_j and t_{on}, without the need of data acquisition with high sample frequency.

In this context, the instantaneous junction temperature is obtained by the convolution of thermal impedance Z_{th} with the power losses, as shown in (3.5) (MA; BLAABJERG, 2012). The thermal impedance is provided by the manufacture datasheet .

$$T_j(t) = T_c + \int_0^t \left[\frac{d}{dz} P_{Loss}(z) \right] .Z_{th}(t - z)dz. \tag{3.5}$$

The initial idea is to obtain the ΔT_j and t_{on} by finding the maximum T_j value, which is achieved with the derivation of (3.5). Thus, in the maximum value of T_j, the heating time and fluctuation junction temperature can be extracted. However, this procedure is not simple, since the power losses waveform has almost sinusoidal shape, which become the mathematical operation complex and time consuming. Thus, one of the most used idea to calculate the ΔT_j in the short-term evaluation is proposed by (MA; BLAABJERG, 2012). This technique estimates the fluctuation temperature approximating the power losses waveform to a two steps square wave pulses with the same area, as showed in Figure 20. As noticed, two different levels of active power injecting by the PV inverter are represented. In both cases, considering the grid frequency equal to fo, the times t_1, t_2 and t_3 are well defined and they have the values of $t_1 = 1/(8f_o)$, $t_2 = 3/(8f_o)$ and $t_3 = 1/(2f_o)$, as discussed in (MA; BLAABJERG, 2012).

When the PV inverter is injecting only fundamental current into the grid, the inverter current is almost perfectly sinusoidal. Thus, the power losses waveform presents basically the same behavior. Moreover, the heating time coincides with the fluctuation junction temperature time. Even though t_{on} is not exactly the same for each range of active power, they are considered constant in order to be applied to the lifetime model. Therefore, the value of t_{on} is fixed in $1/(2fo)$ (REIGOSA et al., 2016).

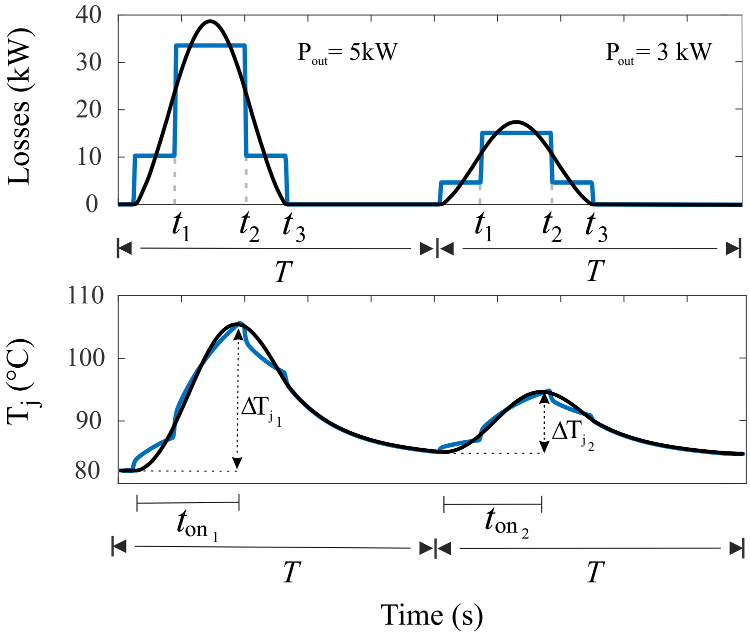

Figure 20 – Conventional methodology with the PV inverter injecting only the fundamental current.

It is relative easy to calculate the temperature fluctuation amplitude considering the power losses from the steps square wave pulses giving by (3.5). Therefore, as proposed by (MA; BLAABJERG, 2012), an analytical equation to estimate the junction temperature fluctuation is showed in (3.6).

$$\Delta T_j = P_{avg}.Z_{th}(t_2) + (3P_{avg} - P_{avg}).Z_{th}(t_2 - t_1). \tag{3.6}$$

where P_{avg} corresponds to the average power loss in one cycle period. All the information of the thermal impedance Z_{th} and the power losses are found in the datasheet manufacture. In addition, the medium junction T_{jm} is directly obtained from the thermal model. Therefore, with ΔT_j, T_j and t_{on} estimation values, these parameters are applied to the lifetime model and the lifetime consumption is calculated, as shown in the flowchart presented in Figure 21.

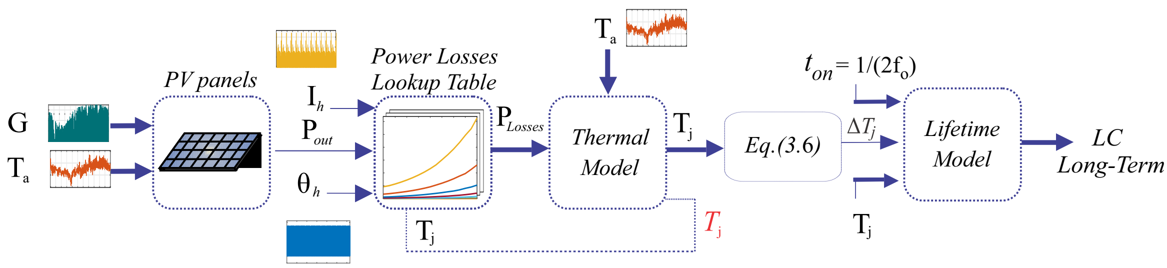

Figure 21 – Flowchart of the lifetime consumption calculation considering the long-term time scale.

It is interesting to note that this technique does not work properly when the PV

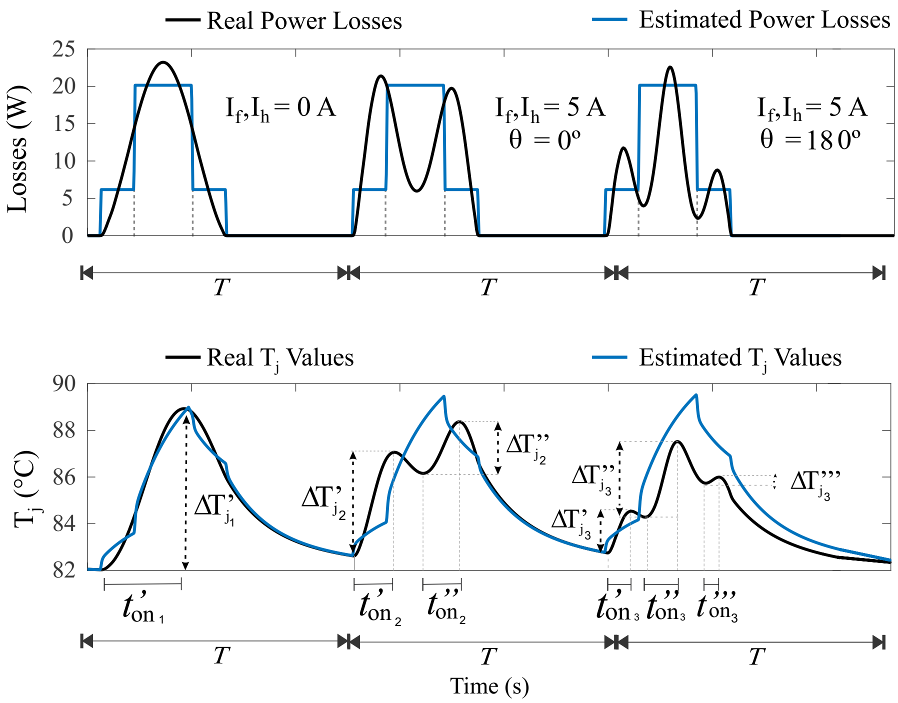

Figure 22 – Conventional methodology when the PV inverter is compensating harmonic current component. For the first cycle, the PV inverter is not working with HCC operation, thus the conventional methodology is applicable. In the second and third cycles, there is a HCC process and the methodology is not applicable.

inverter is compensating harmonic current component, as showed in Figure 22. This fact is explained because the power loss waveform presents a non sinusoidal shape. As noticed, considering a specific harmonic order, the power losses dissipated by the semiconductor device presents characteristics which depend on the θ_h and I_h values. Thus, when the power loss waveform is approximated to a two pulse waveform with the same area, the parameters estimation of ΔT_j and t_{on} are not estimated correctly. Furthermore, there are more than one value of ΔT_j and t_{on} in the same period T. In addition, the medium junction temperature T_{jm} can not be directly estimated using the thermal model, since it has more than one value.

Also, the heating time can not be fixed in $1/(2f_o)$ since the power loss waveform is not sinusoidal. Even if the power losses waveform were approximated by more than two square waveform in order to try to estimate all the ΔT_j and the t_{on}, this technique would be inappropriate, since the power loss waveform has different behavior for each value of harmonic component parameters (h, I_h, θ_h). Thus, this strategy is not adaptive for any parameters of the harmonic current component.

In this scenario, there is a lack of methodologies in the literature to estimate the life consumption when the PV inverter is compensating harmonic current components. In order to fill this void, a proposed short-term methodology, which is able to estimate the LC of semiconductor device under the HCC operation is proposed.

4 New approach for Short-Term lifetime Estimation

This chapter proposes a methodology to estimate the parameters of ΔT_j, T_j and t_{on} when the PV inverter is compensating any current harmonic order. This new technique is adaptive to any harmonic parameter variation of h, I_h, θ_h. In addition, this method avoids the use of analytical equation to estimate ΔT_j and t_{on}, since these parameters are not straightforward to be modeled when the junction temperature shows a non sinusoidal waveform.

Unlike the long-term methodology, this approach is based on a LC lookup table creation, instead of a power loss lookup table. The proposed methodology is described in the following sections.

4.1 Methodology Description: LC Lookup Table Creation

The main goal is making sure that all the parameters of ΔT_j, T_j and t_{on} are considered. Thus, this methodology proposes to extract the lifetime parameters directly from the junction temperature waveform. Therefore, the present study aims to obtain the junction temperature of one cycle and use it to extract all the parameters necessary to the lifetime model. The flowchart for the proposed methodology is presented in Figure 23.

First of all, in a simulation environment, the PV system simulation is performed. For a specific harmonic order, the active power generated by the PV panels, the harmonic current amplitude, the harmonic phase angle and the ambient temperature are varied, for each simulation. Thus, the junction temperature is analyzed.

This methodology demands a steady-state (SS) junction temperature value for a better lifetime consumption estimation. Therefore, T_j is constantly monitored in order to obtain a SS cycle. If the SS is not obtained, the simulation time t_{sim} needs to be increased until the stead state condition be achieved. Otherwise, one cycle of the T_j is stored.

The power cycling due to the switching frequency is not considered. Previous studies have demonstrated that these cycles have a negligible effect on lifetime consumption, since the values of the fluctuation temperature are very small, compared to the power cycling due to the grid frequency (REIGOSA et al., 2016). Therefore, in order to count only the effects caused by the grid frequency, the peaks and valleys of the junction temperature are identified and the information is used to build the SS T_j cycle. Then, this new signal is applied to the rainflow algorithm and the lifetime parameters are obtained.

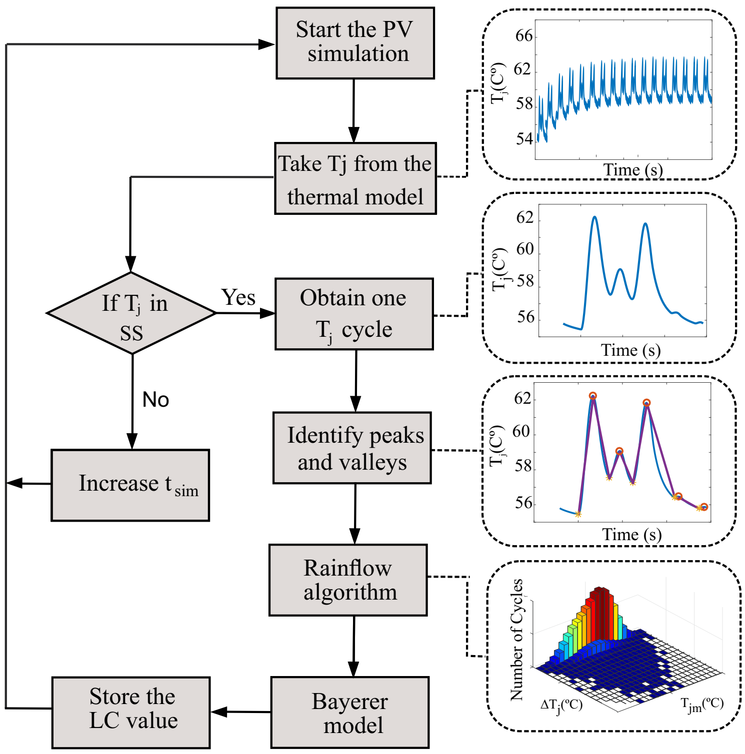

Figure 23 – Flowchat of the proposed short-term methodology: the LC lookup table generation.

Thus, all the parameters of ΔT_j, T_j and t_{on} are estimated and applied to the lifetime model. Then, the LC is calculated and stored in a lookup table, as presented in Figure 24. It is important to observe that this methodology is created for a specific harmonic order. The same procedure can be applied for any harmonic characteristics and their combination. Since the lookup table is generated, the LC can be estimated under one year mission profile. The flowchart for the lifetime consumption, considering the short-term time scale is presented in Figure 25.

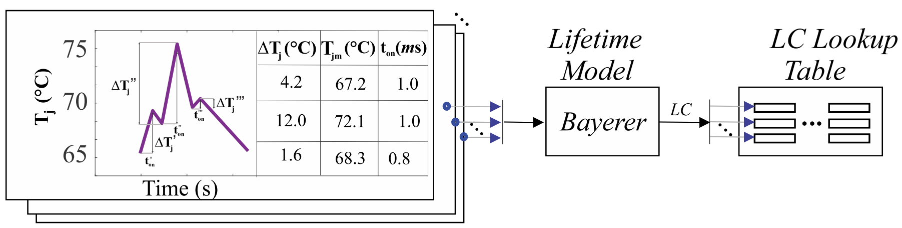

Figure 24 – LC Lookup table creation.

In order to exemplify the proposed methodology, consider the total power loss waveform dissipated in a semiconductor device, as represented in Figure 26(a). Three consecutive cycles are considered. The first cycle, the PV inverter works only with the traditional operation, injecting fundamental current component. In the second and third cycles, the PV inverter injects the 3^{rd} harmonic order with phase angle 0° and 180°,

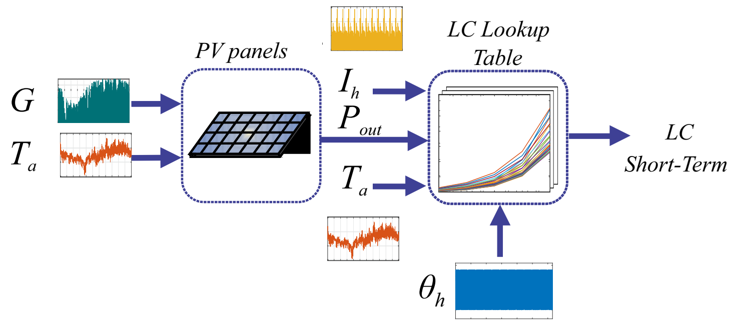

Figure 25 – Flowchart of the LC calculation considering the short-term time scale.

respectively. As noticed, during the HCC process, additional power cycling is added to the power losses and consequently to the junction temperature.

Figure 26(b) shows the estimation of ΔT_j and t_{on} when the methodology proposed by (MA; BLAABJERG, 2012) is employed. As observed, this approximation estimates only one value of the fluctuation temperature and it does not coincide with the real values of ΔT_j. Also, t_{on} estimated only one value and it is fixed in $1/(2f_o)$.

In Figure 26(c), the proposed approach to estimate the short term lifetime parameters is applied to the real junction temperature. As noticed, this technique can take into account all the additional power cycling, due to the HCC operation.

4.1.1 Methodology Validation

In order to analyze the performance of this methodology, the estimation parameters are presented when the PV inverter is compensating the third harmonic component with phase angle equal to 0° and 180°. The semiconductor device used is an IGBT 600V/20A manufactured by Infineon, part number IKW20N60T. In addition, the same study is carried out for the PV inverter working with the traditional operation. As discussed in the previous section, the stress in the power model depends on the ratio of I_h/I_f. Thus, two different values of active power injected by the PV inverter are considered.

In Figure 27 (a), it is considered the junction temperature of the IGBT when the injected active power is 1 kW and the PV inverter works as a traditional operation. In Figure 27(b) and Figure 27(c), it is considered the T_j when the injected active power is also 1 kW, besides, the PV inverter is compensating 5 A of the third harmonic current component with phase 0° and 180°, respectively. The lifetime parameters found by the proposed methodology and the calculated LC are also shown in Table 3. As observed, for high values of I_h/I_f, the waveform of the junction temperature is strongly affected by the harmonic component. In addition, the methodology proposed can achieve all the values of ΔT_j, T_j and t_{on}. For this condition of operation, the LC values for the phase angle equal to 0^o and 180^o are both higher than the LC for a traditional operation of the PV

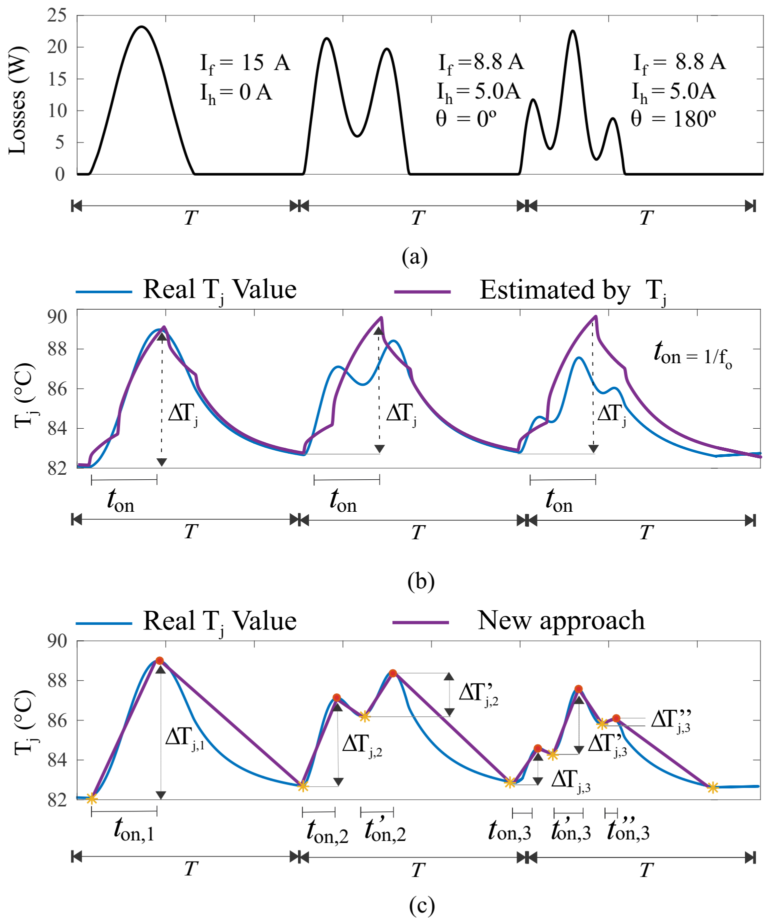

Figure 26 – The total power loss representation of three cycles (a). For the first one, the PV inverter is working as a traditional operation. For the last two cycles, the inverter is operating with HCC. If the traditional methodology is applied, the lifetime parameters estimated are shown in (b). The proposed methodology for short-term is shown in (c).

inverter. Besides, the highest LC value is obtained for the phase angle equal to 180^o, since the values of ΔT_j present the highest values.

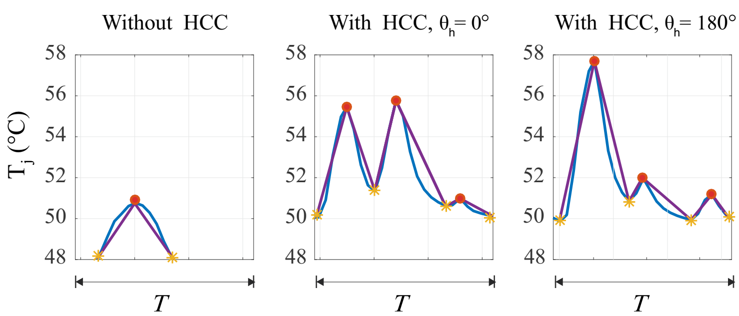

Figure 27 – Performance of the proposed methodology when the PV inverter is injecting: (a) only I_f equal to 4.5 A (1 kW of active power), (b) I_f = 4.5 A, I_h = 5 A and θ_h = 0°, (c) I_f = 4.5 A, I_h = 5 A and θ_h = 180°.

When the PV inverter injects high values of active power, as shown in Figure 28,

Table 3 – Parameters estimation from the proposed methodology for Figure 27.

	ΔT_j (°C)	T_{jm} (°C)	t_{on} (ms)	LC
	4.08	50.51	6.10	
Base Case	-	-	-	2.23 x 10^{-11}
	-	-	-	
	4.95	53.42	3.62	
θ_h=0^o	4.05	54.02	1.83	6.32 x 10^{-11}
	0.52	51.81	0.63	
	6.88	54.53	1.62	
θ_h=180^o	1.71	52.25	1.68	1.22 x 10^{-10}
	0.83	51.75	1.43	

the lifetime parameters and the LC obtained with the proposed methodology are presented in Table 4. As noticed, the LC for phase angle equal to 0^o is even smaller than the one considering the traditional operation of the PV inverter. Also, the LC for θ_h equal to 180^o presents the highest value. This behavior is explained by the lifetime parameters, since ΔT_j has the greatest effect on lifetime consumption calculation. The same idea is used to explain the lowest LC when the θ_h is equal to 0°. Even when it presents higher t_{on} and T_j, compared to the base case, its ΔT_j is the lowest one.

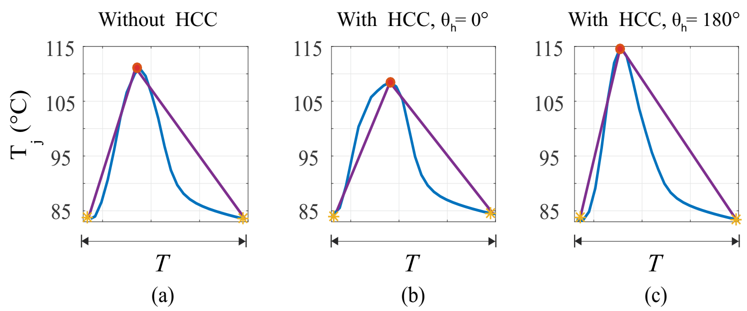

Figure 28 – Performance of the proposed methodology when the PV inverter is injecting: (a) the nominal I_f equal to 22.7A (5 kW of active power), (b) I_f = 22.7 A, I_h = 5 A and θ_h = 0°, (c) I_f = 22.7 A, I_h = 5 A and θ_h = 180°.

Table 4 – Parameters estimation from the proposed methodology for Figure 28.

	ΔT_j (°C)	T_{jm} (°C)	t_{on} (ms)	LC
Base Case	28.12	98.26	6.30	3.82 x 10^{-7}
θ_h=0^o	25.13	97.15	6.40	2.50 x 10^{-7}
θ_h=180^o	29.78	100.31	5.98	1.01 x 10^{-6}

5 Case Study

In this chapter, the lifetime evaluation of a 5kW single-phase PV inverter with HCC operation is performed. Nevertheless, the long-term and short-term time scales are considered in the LC evaluation. The main electrical parameters of the PV system are described in Table 5.

Table 5 – PV system parameters.

Parameter	Value
Nominal Power	5 kW
Grid Voltage	220 V
Dc link Voltage	390 V
Switching Frequency	12 kHz
Sampling Frequency	12 kHz
L_f Filter Inductor	1 mH
L_g Filter Inductor	1 mH
C_f Filter Capacitor	3.8 μC
PCC Voltage	220 V
Grid nominal Frequency	60 Hz

In addition, the power semiconductor device used in this work is a discrete IGBT manufactured by Infineon, part number IKW20N60T. The most important information about the IGBT parameters are presented in Table 6. In order to estimate $R_{eq(h-a)}$, the junction temperature for the nominal operation (when the PV inverter is injecting 5 KW of active power to the grid) was set at 100 °C. Thus, with the equation presented in (3.2), the $R_{eq(h-a)}$ was estimated in 0.6 K/W. In addition, the thermal impedances provided by the datasheet are shown in Table 7.

Table 6 – IGBT main information.

Parameter	Value
V_{CE}	600 V
I_c	20 A
Maximum T_j	175 °C
$R_{eq(j-c)}$	0.9 K/W

Table 7 – IGBT Thermal impedances.

R(K/W)	τ (s)
0.18715	6.92510^{-2}
0.31990	1.08510^{-2}
0.30709	6.79110^{-4}
0.07041	9.59010^{-5}

The data obtained of solar irradiance and ambient temperature over one year are considered. Those data were sampled with one second per data in Alborg (Denmark) from October 2011 to September 2012, as shown in Figure 29. In addition, the data of current harmonic amplitude and phase angle over one year were also sampled with one second per data, as shown in Figure 30.

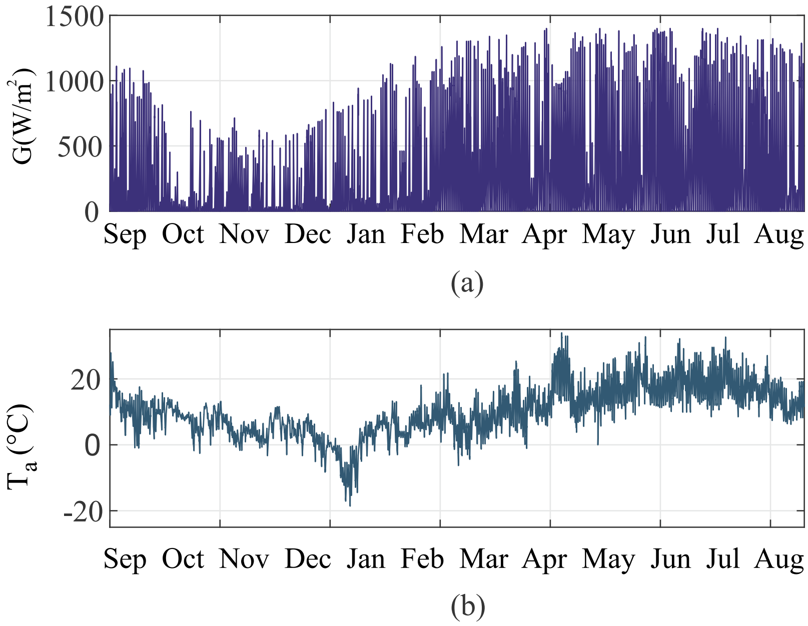

Figure 29 – Mission profile of: (a) solar irradiance and (b) ambient temperature.

In this work, the current distortion composed of a 3^{rd} harmonic order component is considered. The 3^{rd} harmonic order was selected for being very common in single-phase systems. Nevertheless, these values of harmonic phase angle equal to 0° and 180° were selected because they are the extreme values in terms of power losses dissipated in the semiconductor device, as demonstrated in (DE et al., 2018).

The case study is divided in two parts.

Part 1: This part computes the effect on the lifetime consumption due to the HCC operation mode considering the mission profile of the harmonic phase angle. Thus, this value is compared to the traditional PV inverter LC (without the HCC operation).

Part 2: In this part, the harmonic phase angle is set in specific values in order to have a better understand of its relationship with the PV inverter lifetime consumption. The cases in part 2 are described:

- Base Case: Lifetime evaluation in the PV inverter without harmonic current compensation.
- Case 1: Lifetime evaluation of PV inverter compensating the 3^{rd} harmonic component and phase angle equal to 0°.

- Case 2: Lifetime evaluation of PV inverter compensating the 3^{rd} harmonic component and phase angle equal to 180°.

The mission profile of solar irradiance, ambient temperature, harmonic amplitude and phase angle were applied to the three cases and the total lifetime consumption for each case is evaluated.

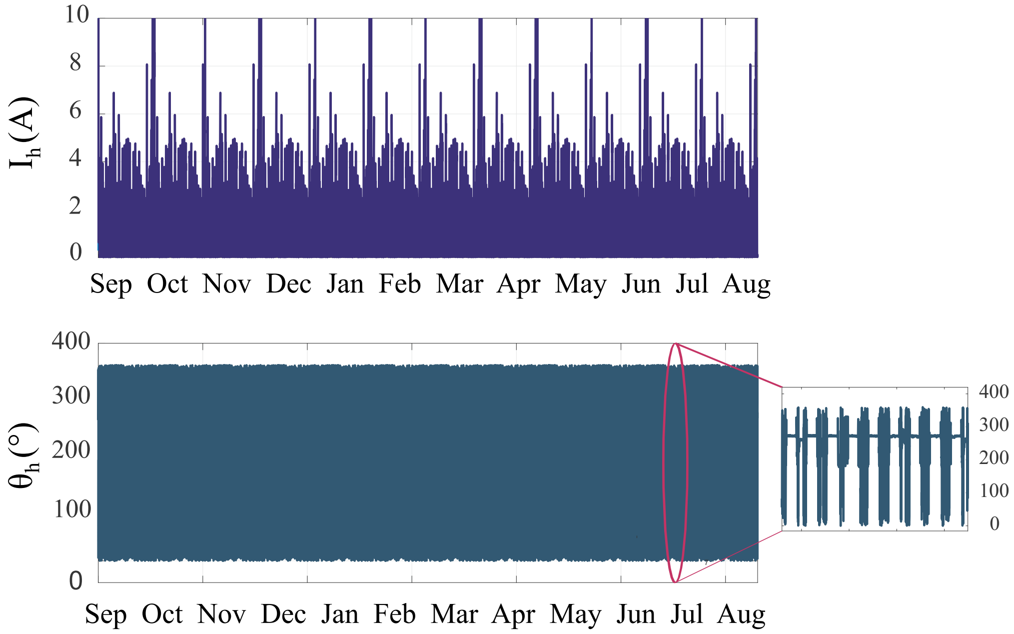

Figure 30 – Mission profile of: (a) harmonic amplitude and (b) phase angle considering only the 3^{rd} harmonic component.

6 Results

The results are divided in two parts, as proposed in the case study. In addition, the short-term and long-term lifetime evaluation are presented in each part. The Monte Carlo analysis considering the unreliability function of the system and component level are also provided.

6.1 Part 1: HCC operation considering variable phase angle.

After the mission profile of solar irradiance, ambient temperature, harmonic amplitude and phase angle over one year be applied to the PV inverter considering HCC operation and using the methodology proposed for the long-term and short-term analysis, the LC are estimated and presented in Table 8. In addition, the same study is made for the PV inverter considering the traditional operation, without HCC operation.

Table 8 – Total lifetime consumption considering short-term and long-term time scales.

Cases	short-term	Long-term	Total
Base Case	0.0266	$1.45\ 10^{-5}$	0.0266
HCC Operation	0.0411	$1.52\ 10^{-5}$	0.0411

As noticed in Table 8, for both cases, the lifetime consumption for long-term is very lower compared to the short-term. Therefore, it is necessary a large quantities of years to cause failures in the semiconductor devices. In this context, the reduction in the lifetime consumption caused by the long-term can be neglected when it is compered to the effects caused by the short-term time scale.

Thus, the total LC is basically the effect caused by the power cycling due to the grid frequency. In addition, it is important to quantify the effect in the PV inverter lifetime consumption caused by the extra functionality of harmonic current compensation. For this reason, the results for the Monte Carlo analysis are presented in Figure 31.

As noticed, when the PV inverter is operating in the HCC mode, the B_{10} value is 24.4 years for the system level and 33.8 years for component level. On the other hand, for the base case, the B_{10} value is 36.9 years for system level and 48.9 years for the component level. It means a lifetime reduction in 33.8 %, considering the system level with HCC operation mode. Thus, these results show the reliability decreasing of the semiconductor device, when the PV inverter is used in the HCC operation.

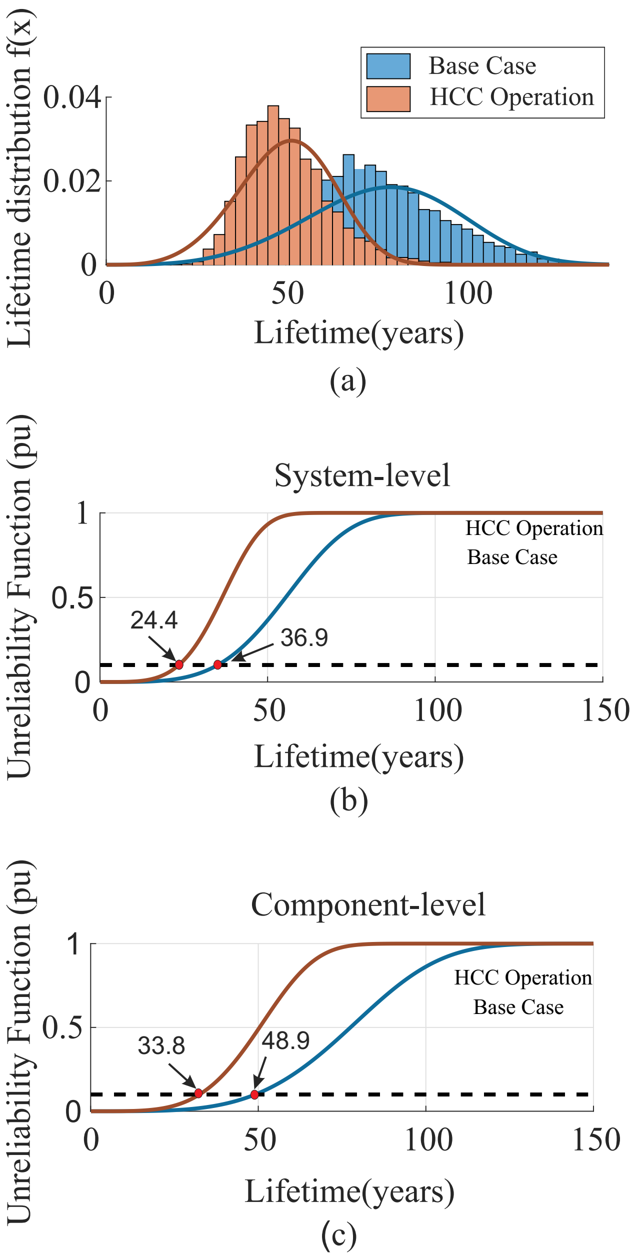

Figure 31 – Lifetime evaluation: (a) lifetime distribution for the two cases (b) unreliability function for system level (c) unreliability function for component level.

6.2 Part 2: HCC operation mode considering fixed values for θ_h.

In this section, the lifetime consumptions for fixed values of 3^{rd} harmonic phase angle is calculated. The 3^{rd} harmonic amplitude is the same presented in Figure 30 (a). Thus, the phase angle is set in fixed value varied from 0° to 360° and the total lifetime consumption over one year for each harmonic phase angle is calculated, as observed in Figure 32.

As observed in Figure 32, the phase angle equal to 180° presents the highest total

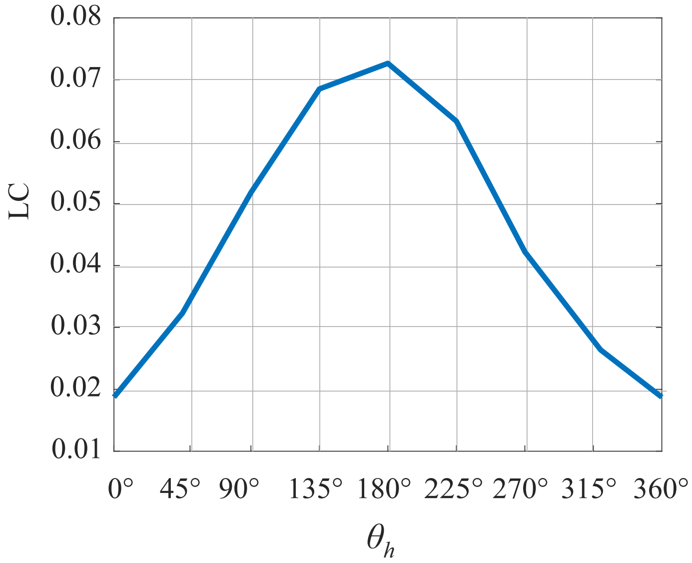

Figure 32 – Total lifetime consumption over one year for different values of harmonic phase angle.

lifetime consumption, equal to 0.0726 % /year. On the other hand, the phase angle 0° presents the lower lifetime consumption, equal to 0.0187 % /year. The short-term and long-term LC for the PV inverter during the HCC operation, considering the phase angle set in 0° and 180°, are presented in Table 9. In addition, the same study is made for the traditional PV inverter, without HCC. In this context, these extreme values of phase angle are selected as a study case in order to apply the Monte Carlo analysis and obtain more details about the effect of the phase angle in the PV inverter reliability.

Table 9 – Total life consumption considering short-term and long-term time scales.

Cases	short-term	Long-term	Total
Base Case	0.0266	1.45 10^{-5}	0.0266
HCC Operation, $\theta_h = 0°$	0.0187	1.49 10^{-5}	0.0187
HCC Operation, $\theta_h = 180°$	0.0726	1.42 10^{-5}	0.0726

As observed in Table 9, when the PV inverter is operating with HCC and the harmonic phase angle is equal to 0°, the LC is 29.69 % lower than that for the base case. On the other hand, when the harmonic current phase angle is 180°, the LC is 172.9 % higher compared to that in the traditional operational of the PV inverter. In addition, the short-term time scale presents a more predominant life consumption compared to that from the long-term. Thus, the total LC is basically the effect caused by the power cycling in the grid frequency time scale. In addition, it is important to quantify the effect on the PV inverter lifetime consumption caused by the extra functionality of the harmonic current compensation. For this reason, the results for the Monte Carlo analysis are presented in Figure 33.

As noticed in Figure 33, when the PV inverter is operating in the HCC mode, the

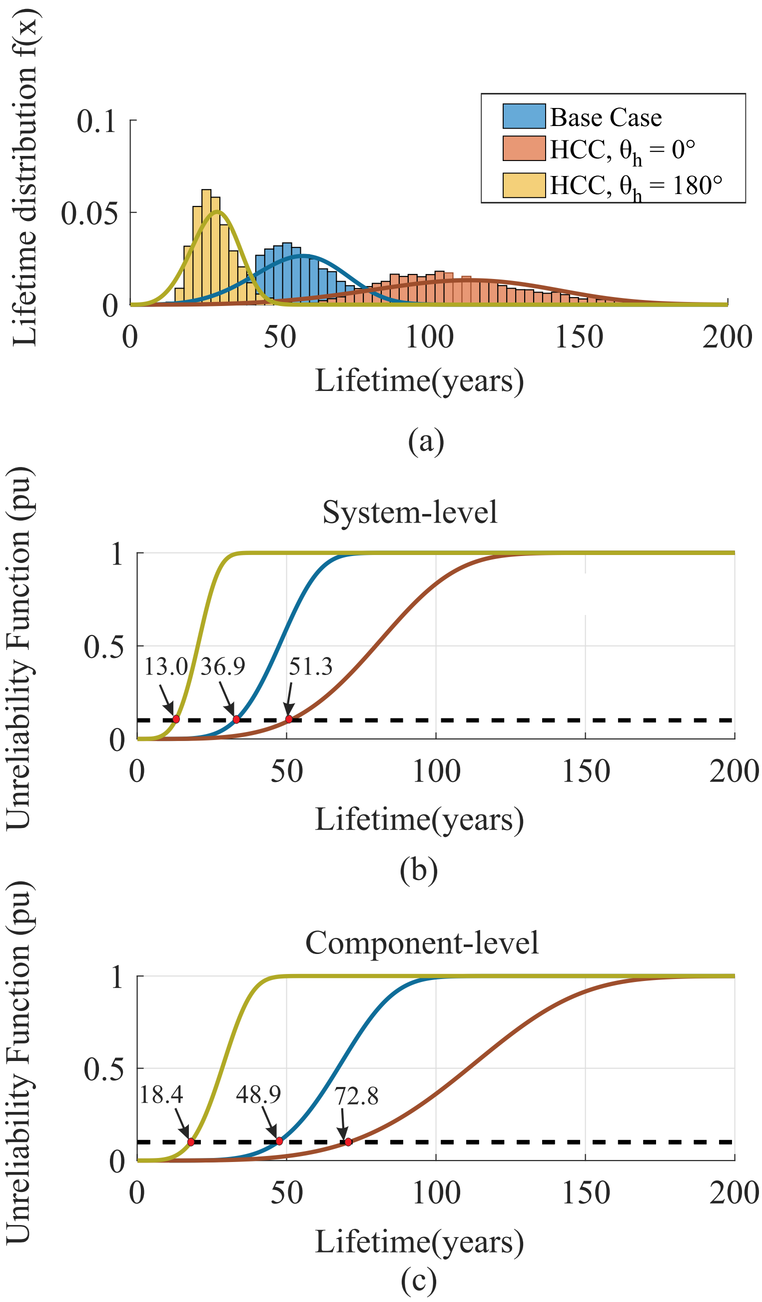

Figure 33 – Lifetime evaluation: (a) lifetime distribution for the three cases (b) unreliability function for system level (c) unreliability function for component Level.

value of the B_{10} analysis for phase angle 0° is 72.8 years for component level and 51.3 years, for the system level. Thus, these results show the increasing reliability of the system level in 39 %, compared to the base case. On the other hand, for phase angle equal to 180°, the value of the B_{10} analysis is 18.4 years for component level and 13.0 years, for the system level. It means a decreasing reliability of the system level in 64%, compared to the base case.

In order to identify the effect caused by the long-term in the IGBT junction temperature, a mission profile of one day is presented in Figure 34. As noticed, for high values of fundamental current (around 12 hour), the junction temperature peak value considering the phase angle 180° is lower in 1.5 °C than that from the base case. On the other hand, for phase angle equal to 0°, the junction temperature is 3.5 °C higher than the base case. In addition, for low values of fundamental current (around 6 hour to 8 hour), both the junction temperature for phase angle 0° and 180° are higher than that from the base case.

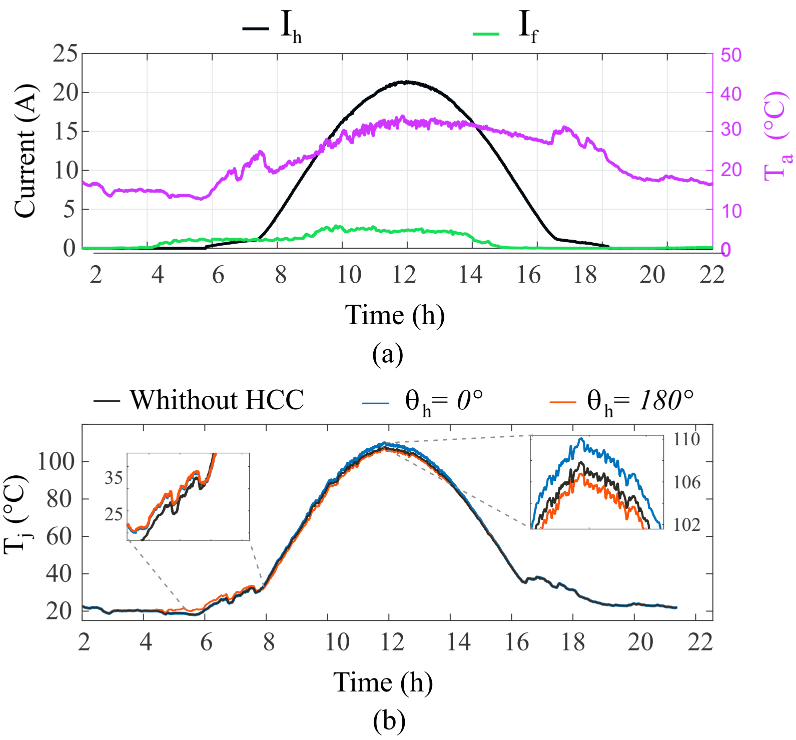

Figure 34 – In (a) is presented the ambient temperature, the fundamental and the 3^{rd} harmonic current amplitude. In (b) are presented the junction temperature considering the phase angle fixed in 0°, 180° and the base case junction temperature.

7 Conclusions

This work proposed to estimate the PV inverter lifetime consumption during the harmonic current compensation process. In this context, the methodology proposed in the literature to estimate the effect of the environmental variation in the PV inverter lifetime consumption was adapted to the HCC operation mode. Nevertheless, regarding the effect of the grid frequency, a new methodology was proposed in this Master's thesis, since there is no work in the literature considering the HCC operation. Thus, a methodology to calculate the LC for the short-term time scale was explored in this work. The methodology can be used for any harmonic component and their different combinations.

The lifetime evaluation of 5 kW PV inverter considering the HCC operation mode is performed. The mission profile of solar irradiance and ambient temperature of a specific place were taken into account. Compared to the traditional PV inverter operation, the results show the decreasing in the PV inverter reliability considering the HCC operation.

Nevertheless, in order to explore the effect of the harmonic phase angle in PV inverter reliability, the LC was performed for the PV system when it is compensating the 3^{rd} harmonic component with phase angle equal to 0° and 180°. It is concluded that the short-term time scale has the greatest effect on the PV inverter life consumption. In addition, compared to the traditional operation of the PV inverter, the LC can be reduced when the PV inverter is compensating the 3^{rd} harmonic component with phase angle equal to 0°. On the other hand, for phase angle equal to 180°, the total lifetime consumption is higher, compared to the traditional PV inverter operation.

In addition, this work developed mathematical equations to calculate the conduction and switching power losses. The equations are adaptive for any harmonic order, amplitude and phase angle. The equations were compared to the power losses obtained from PLECs simulations for different combinations of I_h, θ_h and I_f in order to validate the equations.

References

ANURAG, A.; YANG, Y.; BLAABJERG, F. Reliability analysis of single-phase pv inverters with reactive power injection at night considering mission profiles. *2015 IEEE Energy Conversion Congress and Exposition*, p. 2132–2139, Sept 2015. 26, 28

ASHOUR, H.; YOUSSEF, K. The cost of harmonic losses and mitigations in distribution systems. *International Conference on Electricity Distribution*, v. 28, n. 8, 2005. 25

BARBI, I. Projeto de inversores monofásicos. *Universidade de Santa Catarina*, p. 1–12, Feb 2008. 39, 40, 41, 44

BAYERER, R. et al. Model for power cycling lifetime of igbt modules - various factors influencing lifetime. *5th International Conference on Integrated Power Electronics Systems*, March 2008. 52

BLAABJERG, F. et al. Overview of control and grid synchronization for distributed power generation systems. *IEEE Transactions on Industrial Electronics*, v. 53, n. 5, p. 1398–1409, Oct 2006. 34

BLAABJERG, F. et al. Catastrophic failure and fault-tolerant design of igbt power electronic converters - an overview. *IECON 2013 - 39th Annual Conference of the IEEE Industrial Electronics Society*, p. 507–513, Nov 2013. 27

BRITO, E. et al. Impact of meteorological variations on the lifetime of grid-connected pv inverters. *Microelectronics Reliability*, v. 33, n. 2, p. 1019–1024, Jully 2018. 38, 52

CHEN, K.; STUART, T. A. A study of igbt turn-off behavior and switching losses for zero-voltage and zero-current switching. *Seventh Annual Applied Power Electronics Conference and Exposition*, p. 411–418, Feb 1992. 38, 42

CIOBOTARU, M.; TEODORESCU, R.; BLAABJERG, F. A new single-phase pll structure based on second order generalized integrator. *2006 37th IEEE Power Electronics Specialists Conference*, p. 1–6, 2006. 35

DASH, R.; PAIKRAY, P.; SWAIN, S. C. Active power filter for harmonic mitigation in a distributed power generation system. *2017 Innovations in Power and Advanced Computing Technologies*, p. 1–6, April 2017. 26

DE, R. C. et al. Lifetime evaluation of a multifunctional pv single-phase inverter during harmonic current compensation. *Microelectronics Reliability*, v. 23, n. 5, p. 1071–1076, September 2018. 64

FALCK, J. et al. Reliability of power electronic systems: An industry perspective. *IEEE Industrial Electronics Magazine*, v. 12, n. 2, p. 24–35, June 2018. 13, 26, 27

FEIX, G. et al. Simple methods to calculate igbt and diode conduction and switching losses. *2009 13th European Conference on Power Electronics and Applications*, p. 1–8, Sep. 2009. 38, 40

FERREIRA, V. N. et al. Igbt power modules lifetime in 2-level pv-inverters under harsh environmental conditions. *2017 IEEE 8th International Symposium on Power Electronics for Distributed Generation Systems)*, p. 1–7, April 2017. 27

FILHO, E. M. V. et al. Influence of harmonic distortion in current transformer. *2016 17th International Conference on Harmonics and Quality of Power*, p. 599–604, Oct 2016. 25

GANDHI, O. et al. Reactive power cost from pv inverters considering inverter lifetime assessment. *IEEE Transactions on Sustainable Energy*, p. 1–1, 2018. 28

GHORBANI, S. A. M. Nonlinear loads effect on harmonic distortion and losses of distribution networks. *InternationalPower System Conference*, November 2011. 25

GOLNAS, A. Pv system reliability: An operator's perspective. *IEEE Journal of Photovoltaics*, v. 3, n. 1, p. 416–421, Jan 2013. 27

GOMES A.F. CUPERTINO, H. P. C. C. Damping techniques for grid-connected voltage source converters based on lcl filter: An overview. *Renewable and Sustainable Energy Reviews*, v. 10, n. 4, p. 116–135, Jan 2018. 34

HELD, M. et al. Fast power cycling test of igbt modules in traction application. *Proceedings of Second International Conference on Power Electronics and Drive Systems*, p. 425–430 vol.1, May 1997. 51

HUANG, H.; MAWBY, P. A. A lifetime estimation technique for voltage source inverters. *IEEE Transactions on Power Electronics*, v. 28, n. 8, p. 4113–4119, Aug 2013. 52

IEEE-STD. Ieee recommended practice and requirements for harmonic control in electric power systems - redline. *IEEE Std 519-2014 (Revision of IEEE Std 519-1992) - Redline*, p. 1–213, June 2014. 25

KEXIN, W. et al. Study of bonding wire failure effects on external measurable signals of igbt module. *IEEE Transactions on Device and Materials Reliability*, v. 14, n. 1, p. 83–89, March 2014. 27

KEY, T. Costs and benefits of harmonic current reduction for switch-mode power supplies in a commercial office building. *IAS '95. Conference Record of the 1995 IEEE Industry Applications Conference Thirtieth IAS Annual Meeting*, v. 2, p. 1101–1108 vol.2, Oct 1995. 25

KOLAR, J. W.; ZACH, F. C.; CASANELLAS, F. Losses in pwm inverters using igbts. *IEE Proceedings - Electric Power Applications*, v. 142, n. 4, p. 285–288, July 1995. 42, 43, 44

LIANG, X.; BIN-KARIM, C. A. Harmonics and mitigation techniques through advanced control in grid-connected renewable energy sources: A review. *IEEE Transactions on Industry Applications*, n. 4, p. 3100–3111, July 2018. 25

L.XAVIER. Ancillary services provided by photovoltaic inverters: Single and three phase control strategies. *Computers Electrical Engineering*, v. 7, p. 102 – 12, 2018. 13, 26

MA, K.; BLAABJERG, F. Reliability-cost models for the power switching devices of wind power converters. *2012 3rd IEEE International Symposium on Power Electronics for Distributed Generation Systems*, p. 820–827, June 2012. 53, 54, 59

MA, K. et al. Thermal loading and lifetime estimation for power device considering mission profiles in wind power converter. *IEEE Transactions on Power Electronics*, v. 30, n. 2, p. 590–602, Feb 2015. 28, 49, 50

MA, K.; WANG, H.; BLAABJERG, F. New approaches to reliability assessment: Using physics-of-failure for prediction and design in power electronics systems. *IEEE Power Electronics Magazine*, v. 3, n. 4, p. 28–41, Dec 2016. ISSN 2329-9207. 28

MARSH, G.; WIGNALL, C.; THIES, P. R. Treview and application of rainflow residue processing techniques for accurate fatigue damage estimation. *International Journal of Fatigue*, v. 30, n. 2, p. 757–765, Oct 2015. 51

NERKAR, H.; DHAMAL, S.; SINHA, S. Advanced control technique for solar pv plant to provide ancillary services. *2016 IEEE Region 10 Hu nitarian Technology Conference (R10-HTC)*, p. 1–6, Dec 2016. 26

P-ALZOLA, R. et al. Lcl-filter design for robust active damping in grid-connected converters. *IEEE Transactions on Industrial Informatics*, v. 10, n. 4, p. 2192–2203, Nov 2014. 34

REIGOSA, P. D. Smart derating of switching devices designing more reliable pv inverters. *IEEE Transactions on Industrial Electronics*, November 2014. 28, 37

REIGOSA, P. D. et al. Prediction of bond wire fatigue of igbts in a pv inverter under a long-term operation. *IEEE Transactions on Power Electronics*, v. 31, n. 10, p. 7171–7182, Oct 2016. 28, 49, 52, 53, 57

SANGWONGWANICH, A. et al. Lifetime evaluation of grid-connected pv inverters considering panel degradation rates and installation sites. *IEEE Transactions on Power Electronics*, v. 33, n. 2, p. 1225–1236, Feb 2018. 28, 49

SCHWANZ, D.; BOLLEN, M.; LARSSON, A. A review of solutions for harmonic mitigation. *2016 17th International Conference on Harmonics and Quality of Power*, p. 30–35, Oct 2016. 25

SEKAR, T. C.; RABI, B. J. A review and study of harmonic mitigation techniques. *2012 International Conference on Emerging Trends in Electrical Engineering and Energy Management*, p. 93–97, Dec 2012. 25

SHI, Q. et al. Passive filter installation for harmonic mitigation in residential distribution systems. *2017 IEEE Power Energy Society General Meeting*, p. 1–5, July 2017. 26

SMITH, C. W. Power systems and harmonic factors. *IEEE Potentials*, v. 20, n. 5, p. 10–12, Dec 2002. 25

TODESCHINI, G. Control and derating of a pv inverter for harmonic compensation in a smart distribution system. *2017 IEEE Power Energy Society General Meeting*, p. 1–5, July 2017. 33

Villalva, M. G.; Gazoli, J. R.; Filho, E. R. Comprehensive approach to modeling and simulation of photovoltaic arrays. *IEEE Transactions on Power Electronics*, v. 24, n. 5, p. 1198–1208, May 2009. 50

WEI, K. et al. The igbt losses analysis and calculation of inverter for two-seat electric aircraft application. *The 8th International Conference on Applied Energy*, v. 33, n. 2, Jully 2017. 38

XAVIER, L. S. et al. A novel adaptive current harmonic control strategy applied in multifunctional single-phase solar inverters. *2015 IEEE 13th Brazilian Power Electronics Conference and 1st Southern Power Electronics Conference*, p. 1–6, Nov 2015. 35

YANG K. ZHOU, F. B. Y. Frequency adaptability of harmonics controllers for grid-interfaced converters. *nternational Journal of Control*, November 2015. 34

YANG, Y. et al. Power control flexibilities for grid-connected multi-functional photovoltaic inverters. *IET Renewable Power Generation*, v. 10, n. 4, p. 504–513, 2016. 26

YANG, Y. et al. Pursuing photovoltaic cost-effectiveness: Absolute active power control offers hope in single-phase pv systems. *IEEE Industry Applications Magazine*, v. 23, n. 5, p. 40–49, Sept 2017. 28

ZHOU, L. Effects of wire-bond lift-off on gate circuit of igbt power modules. *Proceedings of 14th International Power Electronics and Motion Control Conference*, p. T1–45–T1–47, Sep. 2010. 27